Blanket and Shielding Considerations for Advanced Tokamak Reactor Concepts

B. Badger, H. Attaya, L. El-Guebaly, G.A. Emmert, J.H. Huang, G.L. Kulcinski, C.W. Maynard, J.F. Santarius, M.E. Sawan, I. Sviatoslavsky, W.F. Vogelsang

December 1983

UWFDM-562

FUSION TECHNOLOGY INSTITUTE

UNIVERSITY OF WISCONSIN

MADISON WISCONSIN

Blanket and Shielding Considerations for Advanced Tokamak Reactor Concepts

B. Badger, H. Attaya, L. El-Guebaly, G.A. Emmert, J.H. Huang, G.L. Kulcinski, C.W. Maynard, J.F. Santarius, M.E. Sawan, I. Sviatoslavsky, W.F. Vogelsang

Fusion Technology Institute
University of Wisconsin
1500 Engineering Drive
Madison, WI 53706

http://fti.neep.wisc.edu

December 1983

UWFDM-562

BLANKET AND SHIELDING CONSIDERATIONS FOR ADVANCED TOKAMAK REACTOR CONCEPTS

Preliminary Report to

Princeton Plasma Physics Laboratory

November 30, 1983

H. Attaya, L. El-Guebaly, G.A. Emmert, J.H. Huang,

G.L. Kulcinski, C.W. Maynard, J.F. Santarius,

M.E. Sawan, I. Sviatoslavsky, W.F. Vogelsang

Fusion Engineering Program
Nuclear Engineering Department
University of Wisconsin-Madison
Madison, Wisconsin 53706

UWFDM-562

ABSTRACT

The design of an inboard shield and outer blanket to handle a peak 10 MW/m^2 neutron wall loading is presented. It is concluded that the inboard superconducting magnets can be shielded with 60 cm of a borated H_2O cooled W/TiH_2/steel shield. Such a shield will protect the Nb_3Sn superconductor while allowing for reasonable heat removal and cryostability criteria to be met. It is shown that a self-cooled Li or $Li_{17}Pb_{83}$/HT-9 steel blanket on the outboard side of a compact tokamak can produce a tritium breeding ratio of more than 1.1 with no breeding required on the inboard side. Preliminary examination of a normal Cu/superconducting hybrid magnet design reveals no particular advantages over the superconducting design.

TABLE OF CONTENTS

1. Introduction and Approach to the Problem

Considerable progress has been made in the past 5 years, both in the physics and engineering aspects of fusion reactors. From the physics community higher beta plasmas, long burn cycles, and impurity removal concepts have been proposed, favorably analyzed, and in some cases even tested. From the technology side, improved materials performance, safer breeder-coolant combinations and more efficient power cycles have made fusion reactors more attractive.

The objective of this study is to apply some of these recent technology advances to the field of compact tokamak research. This preliminary investigation was conducted to see if advances in the following areas justify further analysis:

1. Advanced shielding designs.
2. Advanced blanket designs that reduce the need for inboard breeding.
3. Hybrid superconducting-copper toroidal field coil designs.

1.1 Approach to the Research

Most tokamak reactor designs start with some rather basic assumptions about the desired power level, allowable beta, maximum field at the magnets, and the maximum neutron wall loading that can be handled. These four assumptions then allow the first order dimensions, plasma parameters and requirements for blankets and shields to be calculated. Within these parameters, further detailed analysis produces specific mechanical configurations and power cycles which could be developed. Finally, the cost of the system can be determined as a measure of the success in meeting the original goal of an economically competitive system.

Many scientists and engineers have expressed the concern that at a nominal neutron wall loading of ~ 1 to 2 MW/m^2, the power density in the tokamak is too low to be of economic interest. Therefore, we decided to ask the following question.

> **Assuming that advances in physics will allow a peak neutron wall loading of 10 MW/m^2 to be obtained, how could one design a S/C shield and breeding blanket to take advantage of this condition?**

An auxiliary question which was briefly addressed is:

> **How would the use of a normal copper-superconducting hybrid magnet design change the attractiveness of such a high power density, compact tokamak design?**

The manner in which the first question was approached is outlined schematically in Fig. 1-1.

The main driving parameter in this study was a peak neutron wall loading of 10 MW/m^2 on the inboard side. While the number is somewhat arbitrary, it is indicative of a very high power density system which should enhance the economic viability of the tokamak concept.

The next major task was to set the allowable radiation damage limits for the superconducting coil. The limits for the superconductor, stabilizer, electrical insulation, thermal insulation and heat removal are reviewed in Chapter 2. In some cases we have pushed the conventional limits to allow for progress in the next 5-10 years.

Once the radiation damage limits and peak wall loading were chosen, the design of an optimized inboard shield to protect the S/C coil was initiated. It is worthwhile emphasizing here that a shield to protect against neutron damage is different than that to protect against nuclear heating, radiation damage to insulators, etc. This optimized shield design is described in Chapter 3.

Fig. 1-1

SCHEMATIC OF DESIGN APPROACH

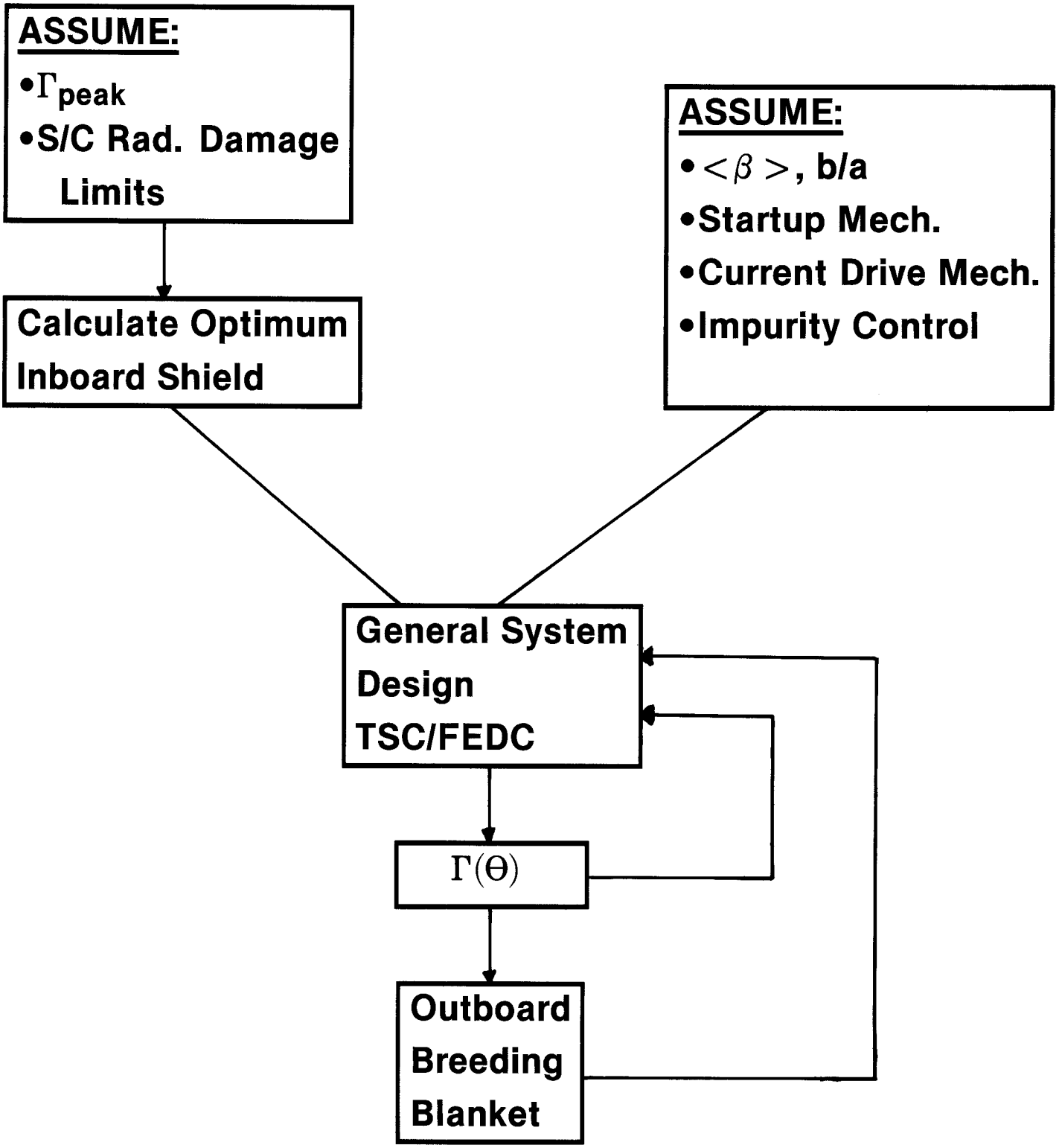

When the optimized shield thickness was obtained, it was inserted into the Tokamak Systems Code (TSC) developed by the FEDC. Other assumptions about the average beta, b/a ratio, mechanisms for startup, current drive, impurity control, etc. were made to develop output power level curves versus aspect ratio for an average 10 MW/m^2 wall loading. This procedure is described in Chapter 4.

The next step is to calculate the poloidal variation in neutron wall loading. This is necessary since the peak wall loading is often 10-20% different than the average value and the poloidal variation is a function of the b/a and aspect ratio. An iterative series of calculations between the poloidal wall loading variation and the TSC was carried out until we obtained a peak wall loading of 10 MW/m^2 on the inboard side of the tokamak. Once this was done, we could make the choice of the power level/aspect ratio combination. Our original desire was to keep the thermal power to below 1000 MW, but to do this at a 10 MW/m^2 peak wall loading required an aspect ratio which was not consistent with our assumption of a high beta. Therefore, we were forced to use power levels in the 1600-1700 MW_{th} range.

The next question faced was could one indeed breed on the outboard side only within the space that was available as well as protecting the outboard leg of the S/C coil? These calculations (see Chapter 5) required only a few iterations to come up with a workable system.

The final question which was addressed pertains to the best use of a normal coil insert (see Chapter 7). For example, it could be used to reduce the field required from the S/C magnet. The objective here would be to allow NbTi operation. The implications of this move are briefly addressed in Chapter 7.

Finally, on the basis of the preliminary analysis, some suggestions for future work are made in Chapter 8. The suggestions cover both the design of compact tokamaks and the areas of research where innovations are required.

2. Limits on Radiation Effects in Superconducting Magnets

A major cost driver in tokamaks is the inboard shield thickness. In a compact tokamak, it is required that this thickness be as small as possible to allow for a high field on axis and consequently high fusion power density. The optimum inboard shield design depends on the different radiation limits for the superconducting magnets. The philosophy in this work is to use the latest information for these limits with possible extrapolation to future performance levels in order to achieve the thinnest possible inboard shield that can protect the magnets from the 10 MW/m^2 neutron wall loading environment. The magnet components most sensitive to radiation in a fusion reactor are the superconductor, the stabilizer and the insulators. To obtain high magnetic fields, the superconductor material was chosen to be Nb_3Sn. The upper critical field at 4.2 K is 22 T for Nb_3Sn and 11.5 T for NbTi. Superfluid helium (LHe-II) at 1.8 K is used as the coolant to allow for use of even higher fields as compared to the case where normal liquid helium (LHe-I) is used at 4.2 K. LHe-II also has the advantage of handling larger heat fluxes.

2.1 Damage to the Superconductor

The most important property for the superconductor is the critical current density (J_c). This gives the maximum current density that it can carry and still remain superconducting. Radiation damage to the superconductor produces defects. The radiation induced changes in J_c depend on the details of the defect structures and their flux pinning capabilities.[1] Unlike NbTi where monotonic decrease in J_c is observed with neutron fluence, an initial increase of J_c with neutron fluence for Nb_3Sn was observed due to enhanced flux pinning.[2] Radiation effects in compound superconductors (Nb_3Sn) differ

considerably from those in alloy superconductors (NbTi) owing to the long-range ordered atomic structure.

Most available experimental data involve irradiating the samples at fission reactor ambient temperatures.[3,4] Experiments performed with irradiation at cryogenic temperatures (5-6 K) showed that the initial J_c increase is larger by ~ 10% than that obtained with samples irradiated at reactor ambient temperatures.[5] This is due to the fact that the defect mobility and subsequent cascade collapse during the high temperature irradiation result in lower flux pinning and a smaller J_c increase. It was also observed that the relative increase in J_c with neutron fluence is larger for higher applied fields.[5] The value of J_c reaches a maximum at fluences of ~ 4 x 10^{18} n/cm^2 (E > 0.1 MeV) and thereafter, a monotonic decrease in J_c with fluence is seen. An 80% increase in J_c with fluence was measured at a field of 10 T after irradiation to a fluence of ~ 4 x 10^{18} n/cm^2 (E > 0.1 MeV) in the High Flux Beam Reactor (HFBR) at 400 K.[3] A larger increase in J_c is expected at the field of 16 T considered in this study.

While room temperature annealing of NbTi results in ~ 70% recovery of the decrease in J_c[1] and hence is beneficial, room temperature annealing of Nb_3Sn results in recovering the initial increase in J_c by irradiation. This recovery increases with field. This implies that annealing of high field Nb_3Sn magnets should be avoided. Hence, the maximum allowable neutron fluence should not be reached until the end of life of the magnet. A lifetime fluence limit of 4 x 10^{18} n/cm^2 (E > 0.1 MeV) (~ 0.002 dpa) has been quoted by different researchers.[3,6] This corresponds to the fluence at which the change in J_c is zero at an applied field of 10 T (the point where J_c is maximum). However, the experimental results show that J_c drops to its pre-

irradiation value at a fluence of ~ 10^{19} n/cm^2 (E > 0.1 MeV).[3] This implies that higher fluences can be used without degrading J_c much below its original unirradiated value. In this work we use a fluence limit of 4 x 10^{19} n/cm^2 (E > 0.1 MeV) (~ 0.02 dpa) which is an order of magnitude higher than the quoted limit. This is based on the prediction that the higher fields and lower temperatures used in this design will result in large initial increases in J_c with irradiation. Furthermore, the effect of heat treatment of the Nb_3Sn superconductor filaments has not been investigated. Extensive studies on the effect of heat treatment on J_c for NbTi have indicated that cold work develops fine scale, heterogeneous microstructure that pins fluxoids effectively and enhances J_c.

2.2 Damage to the Stabilizer

Most designs for fusion magnets have adopted the conservative principle of cryogenic stabilization. The stabilizer is used to provide an alternate low resistance path for the current when a part of the superconductor is driven normal by any instability. A low stabilizer resistivity is required such that the resistive heat (I^2R) produced by the current flowing in it can be removed by the coolant and the temperature kept below the critical temperature for the superconducting mode to resume. The resistivity of the stabilizer at the operating magnetic field and temperature is, therefore, the important parameter.

Neutron irradiation at cryogenic temperatures produces immobile point defects in the stabilizer which decrease the mean free path of the conduction electrons resulting in a radiation induced resistivity $\Delta\rho_r$. This radiation induced resistivity, which is related to damage in the stabilizer, must there-

fore be limited to a maximum value for the magnet to be cryostable. The upper limit on the total resistivity at the field B is given by

$$\rho_{max}(B) = q''_{max} A_{st} P/I^2 \ , \qquad (2.1)$$

where A_{st} is the stabilizer cross section area, P is the wetted perimeter and I is the conductor current. q''_{max} is the maximum heat flux that can be removed by the coolant. It is clear that the resistivity limit depends on the magnet design parameters.

Copper and aluminum are the two stabilizer candidates. Because of its strength, fabricability and small radiation induced resistivity, copper appears to be the favored material. Determination of the dpa rate limit in Cu is complicated by the dependence of the resistivity at the operating field on the radiation induced resistivity and the purity of Cu. This dependence is usually represented by the Kohler plot.[7] Furthermore, partial recovery (80-90%) of radiation induced defects can be achieved by room temperature annealing.[8]

We have generated charts for determining the maximum allowable damage rate in copper stabilizer.[9] An algorithm for determining the dpa rate limit for given magnet design and reactor availability requirements is summarized in the flow chart of Fig. 2-1. The charts used to determine the limit on radiation induced resistivity and the minimum time before the first magnet anneal are given in Figs. 2-2 and 2-3, respectively.

In this design we assume a maximum S/C current density of 8×10^4 A/cm^2. This is based on assuming a critical current density of 10^5 A/cm^2 at 16 T and 1.8 K and an 80% safety factor. The Cu:S/C ratio is taken to be 16:1 and the

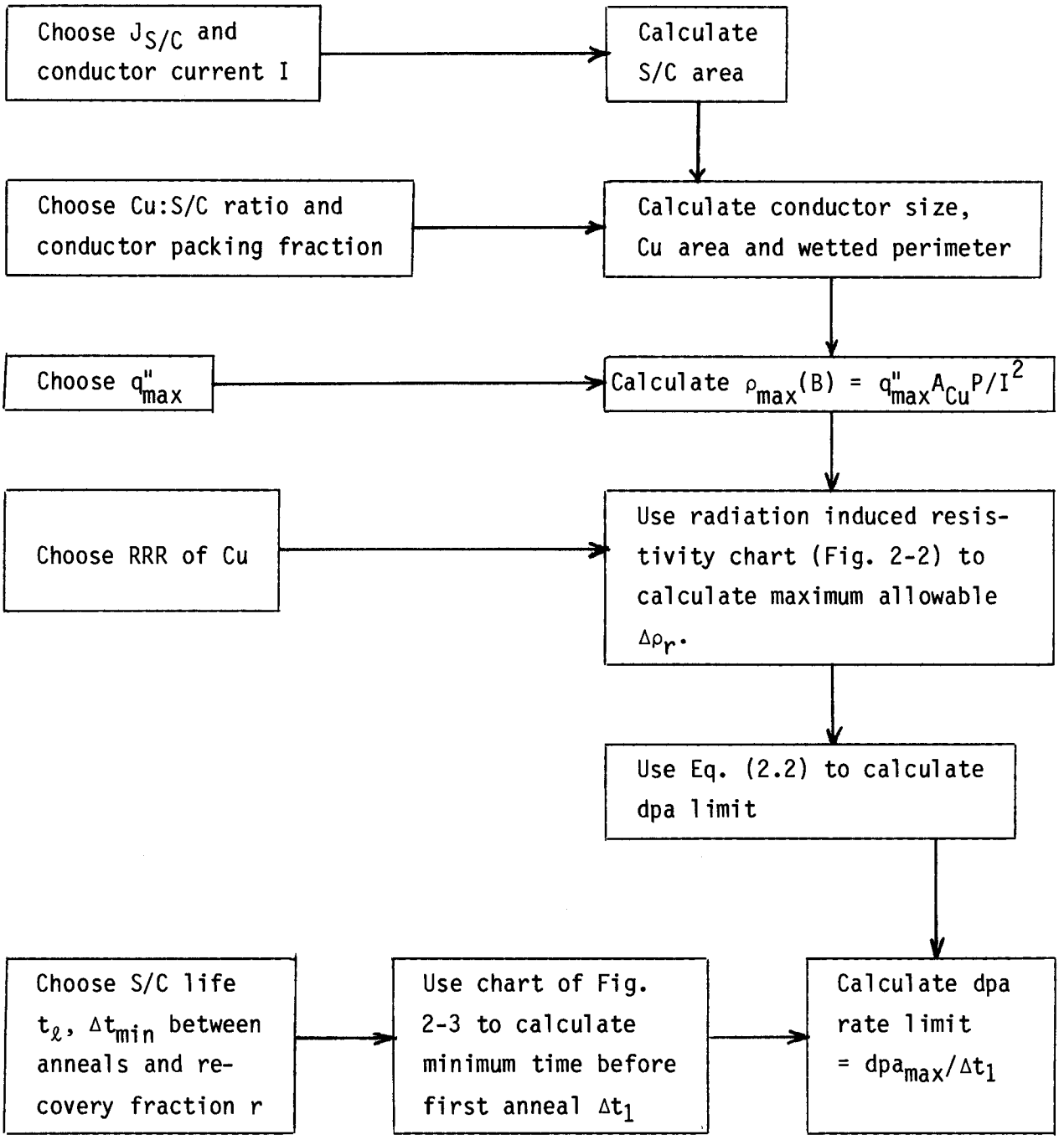

Fig. 2-1. Flow chart for calculating dpa rate limit in Cu.

Fig. 2-2. Radiation induced resistivity chart for Cu.

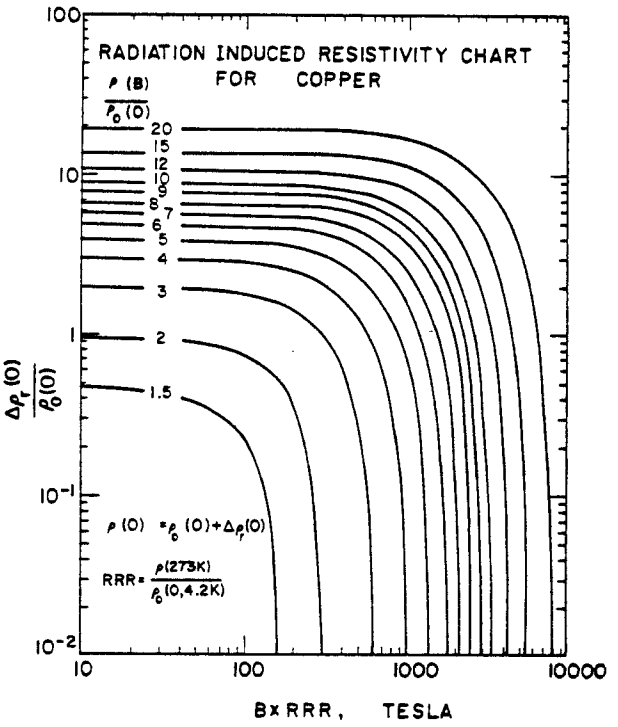

Fig. 2-3. Chart to determine minimum time required before first magnet anneal.

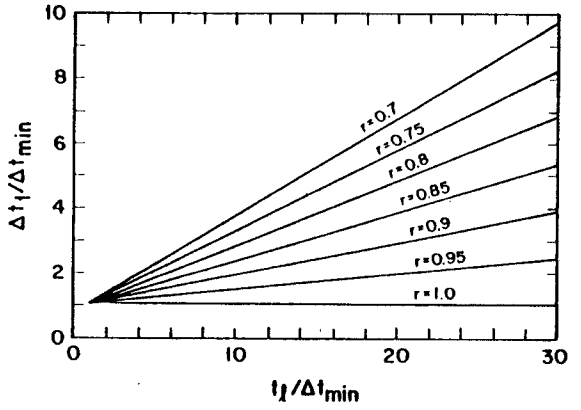

conductor packing factor is assumed to be 85%. This implies an average winding pack current density of 4000 A/cm^2. The conductor is assumed to have a square cross section with 50% of the conductor perimeter being wetted by the LHe-II coolant.

According to Hoard[10] and Parmer,[11] LHe-II can handle a heat flux of up to 2.37 W/cm^2. The coolant must be able to remove not only the I^2R heat produced in abnormal conditions but also the continuous heat production resulting from nuclear heating in the magnet. Hence, the value of q''_{max} used in Eq. (2.1) should be less than 2.37 W/cm^2 to allow for a margin that can handle nuclear heating. In this study, we considered values of 1, 2, and 2.37 W/cm^2 for q''_{max} to investigate its impact on dpa rate and nuclear heating limits. Half hard Cu with a residual resistivity ratio RRR = 80 is considered here. The relation between $\Delta\rho_r$ and Cu dpa is taken to be

$$\Delta\rho_r = 300\left[1 - e^{-240\ \text{dpa}}\right]\ n\Omega\ \text{cm}\ . \qquad (2.2)$$

It was obtained by Guinan et al.[12] using the neutron spectrum at the MARS[13] central cell S/C coils.

Originally, we assumed an operating current in the conductor of 10 kA yielding a conductor size of 1.46 cm. Assuming the maximum heat flux to be 2.36 W/cm^2, Eq. (2.1) yields $\rho_{max}(B)$ = 138 nΩ cm. Using the chart in Fig. 2-2 implies that the radiation induced resistivity should not exceed 38.6 nΩ cm. This relatively low limit on radiation induced resistivity is due to the large Cu magnetoresistivity at 16 T. Using Eq. (2.2) gives a dpa limit of 5.74 x 10^{-4}. The reactor life was assumed to be 24 FPY. The minimum time between magnet anneals determined from availability considerations was set to be

1 FPY. Assuming a recovery fraction of 0.85, the chart in Fig. 2-3 indicates that the time before the first magnet anneal should be at least 4.45 FPY and eleven magnet anneals will be needed during the 24 FPY reactor life. This implies that the dpa rate should not exceed 1.3×10^{-4} dpa/FPY if an operating conductor current of 10 kA is used. The 60 cm thick optimized shield that gives a neutron fluence at the S/C of 4×10^{19} n/cm^2 (E > 0.1 MeV) was found to yield a dpa rate of 1.2×10^{-3} dpa/FPY in the Cu stabilizer. This implies that the magnet will not be unconditionally cryostable if a conductor current of 10 kA is used even with the limit on the heat flux being pushed to 2.36 W/cm^2.

There are several options to remedy this situation. One can rely on end zone stabilization where the conductor can recover by heat transfer along the conductor axis. Other stabilization mechanisms such as adiabatic stabilization can be considered. Another possibility is using Al stabilizer because of its much smaller magnetoresistivity. However, Al has a much larger radiation induced resistivity for the same neutron fluence (saturation resistivity is 800 nΩ cm versus 300 nΩ cm for Cu). Furthermore, extra structure is needed to provide strength which reduces the stabilizer area or increases the coil cross section area. Preliminary calculations indicate that Cu is preferable to Al in this design. However, detailed trade-off studies are needed to investigate the possibility of using Al instead of Cu in the high field coils.

If unconditional cryostability is required without increasing the inboard shield thickness, it will be necessary to reduce the conductor current and conductor size. This is equivalent to dividing the conductor into several smaller conductors to enhance the cooled area. The total coil cross sectional area remains the same. Table 2-1 gives the maximum conductor current and size

Table 2-1. Conductor Parameters Required for Cryostability With a Peak dpa Rate of 1.2×10^{-3} dpa/FPY

Maximum heat flux (W/cm^2)	1	2	2.36
Maximum conductor current (A)	337	1348	1877
Maximum conductor size (cm)	0.27	0.54	0.63

that can be used for the magnet to be cryostable with a peak dpa rate of 1.2×10^{-3} dpa/FPY. The values corresponding to different heat flux limits are given. Such small conductor sizes can be achieved by designing a braided conductor with a small current flowing in each braid. The braided conductor can be placed in a steel jacket. Such a design is possible based on experience with the Westinghouse Nb_3Sn LCP forced flow conductor.[14]

It is interesting to note that Eq. (2.2) implies a saturation value of 300 nΩ cm for the radiation induced resistivity in Cu. Hence, if the magnet is designed such that the coolant can remove the I^2R heat produced by the residual resistivity, magnetoresistivity, and the saturation radiation induced resistivity, it will be unconditionally cryostable regardless of the amount of damage produced in the stabilizer. In such a design, no limit needs to be specified for the dpa rate and no magnet annealing will be necessary. The maximum required conductor current and size are given in Table 2-2. A maximum heat flux of 2 W/cm^2 resulting from the I^2R heating in the stabilizer will be considered in this study leaving a margin of 0.37 W/cm^2 for nuclear heating. Comparing Tables 2-1 and 2-2, it is clear that the limit on dpa rate can be removed completely by a small reduction in conductor size and current. Therefore, a conductor 0.44 x 0.44 cm in size which carries 900 A was chosen for

Table 2-2. Conductor Design Parameters Required for the Magnet To be Cryostable with Unlimited Stabilizer dpa

Maximum heat flux (W/cm^2)	1	2	2.36
Maximum conductor current (A)	225	900	1253
Maximum conductor size (cm)	0.22	0.44	0.52

this design. This will eliminate the need for magnet annealing which is beneficial for Nb_3Sn as it was found that room temperature annealing reduces the initial increase in critical current density with neutron fluence. It should also be noted that the largest damage to the stabilizer occurs only in the innermost layers of the coil. Also the field drops in the outer layers of the coil. Hence, a graded coil can be used with larger conductor sizes and currents used in the outer grades.

2.3 Nuclear Heating Limit

The heat flux margin that can be used by nuclear heating is 0.37 W/cm^2. For the chosen conductor parameters, this corresponds to a volumetric power density of 1430 mW/cm^3. This is the maximum allowable peak power density in the winding pack resulting from nuclear heating. This is a very large value and does not impact the shield design. However, much lower power densities are required to avoid excessively high cryogenic refrigeration and plant cost. The 60 cm thick optimized shield used in this study yields a peak power density of 2.2 mW/cm^3. Since the power density decreases as one moves towards the outer layers of magnet and these high power densities are obtained only on the inboard section of the coil where limited shielding space is available, this

does not result in excessive cryogenic heat load. The total power generated in the inboard sections of the twelve coils is ~ 4 kW.

2.4 Dose Limit to the Insulators

The insulators are intended to carry the Lorentz forces on the conductors, provide space for liquid helium coolant, and prevent shorting or breakdown between turns of the magnet or to the magnet case. The strength and resistivity of the insulators are the important properties. Experimental data for fiber-reinforced organic insulators indicate that the mechanical properties degrade at a lower dose than do the electrical ones.[6]

Mechanical strength tests of irradiated magnet insulators have shown that polyimides are 5 to 10 times more radiation resistant than comparably prepared epoxies.[15] These results indicate that more than 65% of the compression strength of glass filled fiber (gff) polyimide is retained up to a dose of ~ 10^{10} rad. In these experiments, samples of several millimeters thick cylindrical rods of polyimide were gamma irradiated at 5 K and the mechanical properties (flexural and compression strengths) were determined at 77 K and 300 K. The samples are representative of relatively thick sheets of insulators placed between conductors. Both compression and interlaminar shear are important in this mode of application of the insulator materials.

Recently, thin disks of gff epoxies and polyimides were irradiated at 325 K and tested at room temperature. The disks are 0.5 mm thick and 11.1 mm in diameter.[16] These are representative of the case when thin sheets of insulators are sandwiched between large conductor plates and held in compressive load only. The samples were irradiated to mixed gamma and neutron doses of ~ 4 x 10^{11} rads. Static compression tests were made to a maximum stress level of 2750 MPa with no failures observed. This indicates that dose limits of ~ 4

x 10^{11} rads can be used for the polyimide insulator provided it is used in the form of thin disks loaded in compression only. The insulator may have to be a composite of thin sheets of insulator sandwiched between metal plates. Helium flow channels could be cut into this composite material and the shear stresses could be borne by the metallic component.[17] In this study, a gff polyimide is used as electrical insulator. The end of life dose limit for the insulator is taken to be 4 x 10^{11} rad.

Aluminized mylar has been used in previous designs as superinsulator (thermal insulator). However, recent experiments showed a large drop in its strength after irradiation to 6 x 10^{8} rads.[18] No failure of any type was observed in aluminized Kapton up to a dose of 10^{10} rads implying that they can serve as superinsulation at these doses.[19] The superinsulator is located in front of the magnet case and is, therefore, exposed to doses higher than those in the electrical insulators. It is, therefore, essential to use a superinsulator that can stand higher radiation doses. For this reason aluminum sheets supported with glass paper are used for superinsulation in the inboard side in this study. These are believed to stand very high radiation doses. Aluminized Kapton can be used in the outboard side where large shielding space is available.

References for Chapter 2

1. B. Brown, J. Nucl. Mat. 97, 1 (1981).
2. C. Snead, Jr. and D. Parkin, Nucl. Technology 29, 264 (1976).
3. C. Snead, Jr. et al., J. Nucl. Mat. 103 & 104, 749 (1981).
4. D. Parkin and D. Schurtzen, Nucl. Technology 22, 108 (1974).
5. B. Brown et al., J. Appl. Phys. 49, 4144 (1978).

6. R. Van Konynenburg and M. Guinan, "Relative Radiation Sensitivity of Insulators, Stabilizers, and Superconductors," UCID-19292, Lawrence Livermore Laboratory Report (1982).

7. F. Fickett, "Magnetoresistivity of Cu and Al at Cryogenic Temperatures," Proc. 4th Intl. Conf. Magnet Technology, CONF-720908, pp. 539 (1972).

8. B. Brown et al., J. Nucl. Mat. 52, 215 (1974).

9. M. Sawan, "Charts for Specifying Limits on Copper Stabilizer Damage Rate," Proc. 3rd Top. Mtg. on Fusion Reactor Materials, Albuquerque, NM, Sept. 1983.

10. R. Hoard, "Heat Transfer and Stability of TMNS coils in Superfluid He-II," LLNL Memo, Feb. 1981.

11. J. Parmer, "Conductor Design for Superfluid He-II," 1982 Applied Superconductivity Conf., Knoxville, TN.

12. M. Guinan et al., "Defect Production and Recovery in FCC Metals Irradiated at 4.2 K," Proc. 3rd Top. Mtg. Fusion Reactor Materials, Albquerque, NM, Sept. 1983.

13. B. Logan et al., "The Mirror Advanced Reactor Study (MARS) Final Design Report," UCRL-53333-83, Lawrence Livermore Lab. (1983).

14. P. Sanger et al., "Design Considerations for the Nb_3Sn Forced Flow Conductor for LCP," Proc. 7th Symp. on Engineering Problems of Fusion Research, IEEE publication #77CH1267-4-NPS, pp. 948 (1977).

15. R. Colman and C. Klabunde, J. Nucl. Mat. 103 & 104, 717 (1981).

16. R. Shmunk et al., "Tests on Irradiated Magnet Insulator Materials," Proc. 3rd Top. Mtg. on Fusion Reactor Materials, Albuquerque, NM, Sept. 1983.

17. K. Agarwal, General Dynamics, private communications (July 1983).

18. S. Takamura and T. Kato, J. Nucl. Mat., 103 & 104, 729 (1981).

19. C. Long et al., "Effects of Radiation at 5 K on Organic Insulators for Superconducting Magnets," Special Purpose Materials Progress Report, U.S. DOE Report DOE/ER0004811, pp. 73 (1981).

3. Inboard Shield Design

The radiation effects of concern in the superconducting (S/C) magnet are the nuclear heat load, the atomic displacement (dpa) rate in the stabilizer, the fast neutron fluence in the superconductor, and the dose to the insulators. The inboard part of the S/C magnet is operating in a severe radiation environment and is designed for high performance (high magnetic field, high current density, etc.). The limited space available for the inboard shield to protect the S/C magnet from the intense neutron source (10 MW/m^2 wall loading) strongly suggests the need for a shield optimization study to minimize the four most important responses mentioned above.

The S/C magnet is superfluid helium (He-II) cooled to withstand the high heat load and allow for the large magnetic field required to produce high fusion power density. It utilizes highly radiation resistant electrical and thermal insulators, namely the GFF polyimide and the glass-paper supported Al sheets, respectively. The production of the high magnetic field (16 T at the coil) mandates the use of Nb_3Sn as the superconductor. The S/C magnet shielding requirements are set by a number of radiation limits (see Chapter 2).

In summary, the peak dose in the GFF polyimide was taken as 4×10^{11} rad after the 24 FPY reactor life. The limit on the nuclear heat load in the S/C magnet is design-dependent. Although winding pack peak power densities as large as ~ 1 W/cm^3 can be tolerated by the He-II cooling system, much lower power densities are preferable to avoid excessively high cryogenic plant cost and power. To avoid degradation of the critical current density for the superconductor material, the peak neutron fluence (for $E_n > 0.1$ MeV) in the S/C magnet should not exceed 4×10^{19} n/cm^2 at the end of the reactor life. The conductor is designed in a way that allows the magnet to be uncondi-

tionally cryostable regardless of the damage produced in the stabilizer as explained in Section 2.2. This implies that no upper limit on the dpa rate needs to be specified and no magnet annealing is required during the reactor life.

3.1 Shield Optimization

The primary motive for the optimization study is to find an optimal combination of the shielding materials that minimizes the fast neutron fluence in the S/C magnet which was found to be the design driver for the shield. The S/C magnet and its associated cryostat are represented schematically by Fig. 3-1 for the preliminary case of the reactor design where the major radius, minor radius, and winding pack radial thickness are 3.07, 0.55 and 1.07 m, respectively. A space of 0.17 m was reserved for the cryostat and the shield was constrained to 0.8 m. In this regard, the use of tungsten in the shield is essential to provide adequate protection for the S/C magnet.

A series of one-dimensional (1-D) calculations was performed to determine the optimal shield configuration using the discrete ordinates code ONEDANT,[1] the cross section library XSLIB (30 neutron and 12 gamma energy groups) based on the ENDF/B-V evaluation, and the P_3-S_8 approximation, in cylindrical geometry with the reactor centerline as an axis. The shield was configured originally in two layers: first, a W-shield (80 vol.% W [95% d.f.], 10 vol.% Fe-1422, and 10 vol.% H_2O) to effectively attenuate the high energy neutrons, and next, a titanium hydride (TiH_2)-shield (80 vol.% TiH_2, 10 vol.% Fe-1422, and 10 vol.% H_2O). One good feature about the TiH_2 is its high hydrogen content (40% more than in H_2O) which helps in further moderating the neutrons via elastic scattering interactions. The steel content in the shield was kept at

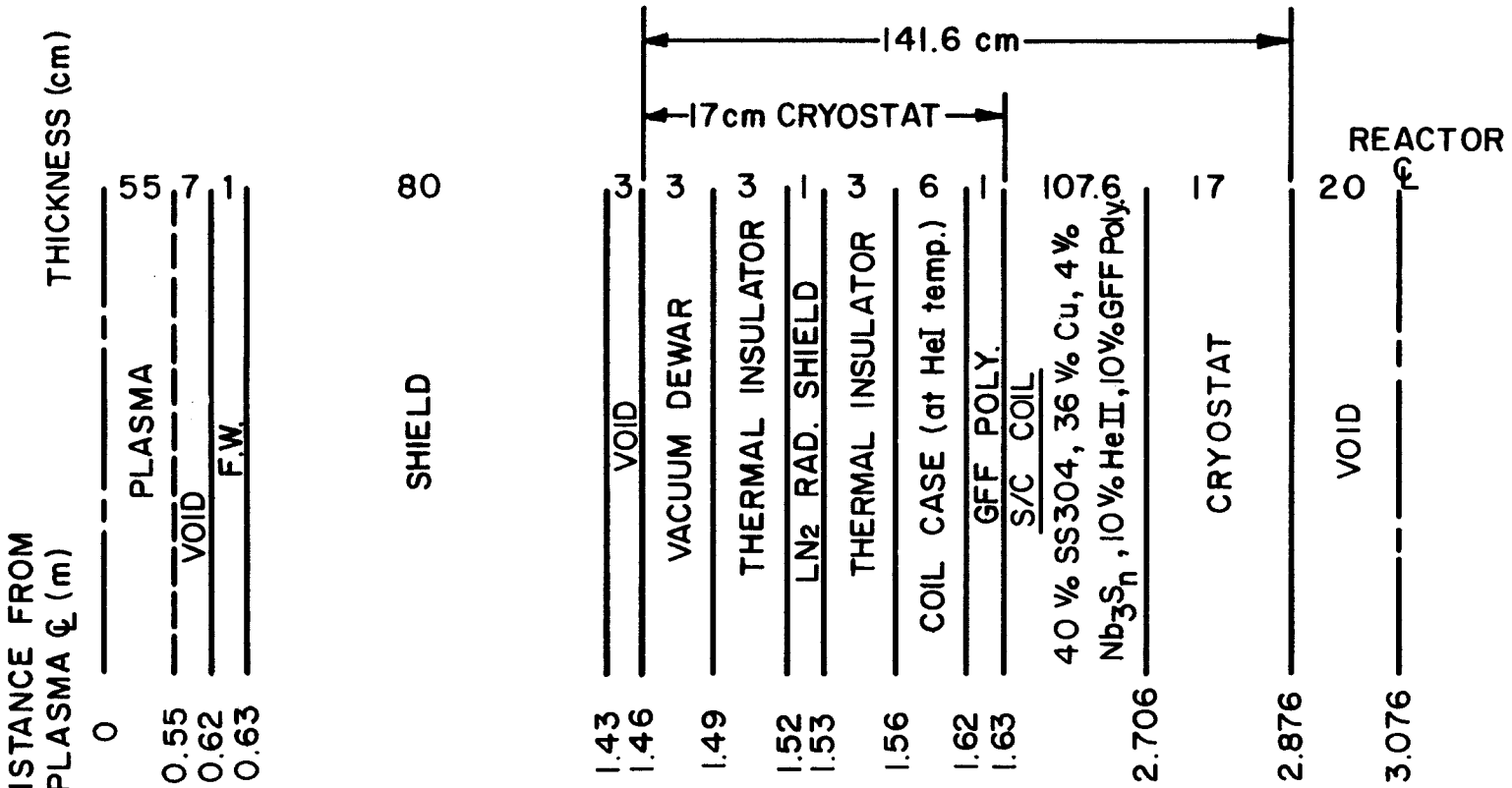

SCHEMATIC OF THE INBOARD SHIELD AND S/C MAGNET FOR THE PRELIMINARY DESIGN

Fig. 3-1. Schematic of the inboard shield and S/C magnet.

the 10 vol.% minimal value and the water content was varied in the optimization study as will be shown later.

The optimization study was performed in several steps. The TiH_2-shield was varied in thickness under the constraint that the total shield thickness remain 0.8 m. Figure 3-2 indicates that 0.72 m of W-shield backed by 0.08 m of TiH_2-shield is the optimal combination that minimizes the fast neutron fluence in the conductor. The effect of the water content in the shield on the fluence is shown in Fig. 3-3. This reveals that as little water as possible is required and in order to meet the cooling demands for the shield, a 10 vol.% coolant content was considered. This choice also has the beneficial effect of reducing the peak power density in the S/C magnet. An attempt was made to further reduce the nuclear heating without substantially affecting the fast neutron fluence in the S/C manget. Boric acid (H_3BO_3 with 90% ^{10}B in B) was added gradually to the water to absorb the low energy neutrons, and its effect is shown in Fig. 3-4. As anticipated, it barely affects the fast neutron fluence but reduces the power density considerably. The solubility of boric acid in water has a strong temperature dependence. For an inlet coolant temperature of ~ 100°C in the inboard shield, the maximum allowable concentration of boric acid in water is ~ 11 vol.%.[2] This corresponds to a 25% reduction in the power density.

The option of using lead and boron carbide to back up the shield was also considered. The effect of the Pb-shield (80 vol.% Pb, 10 vol.% Fe-1422, and 10 vol.% H_2O) in a 0.8 m thick shield is shown in Fig. 3-5, where the W and TiH_2-shield thicknesses were reduced (but their ratio was kept the same) and several centimeters of Pb-shield were added at the back. As indicated in the figure, the Pb-shield is effective in reducing the power density in the S/C

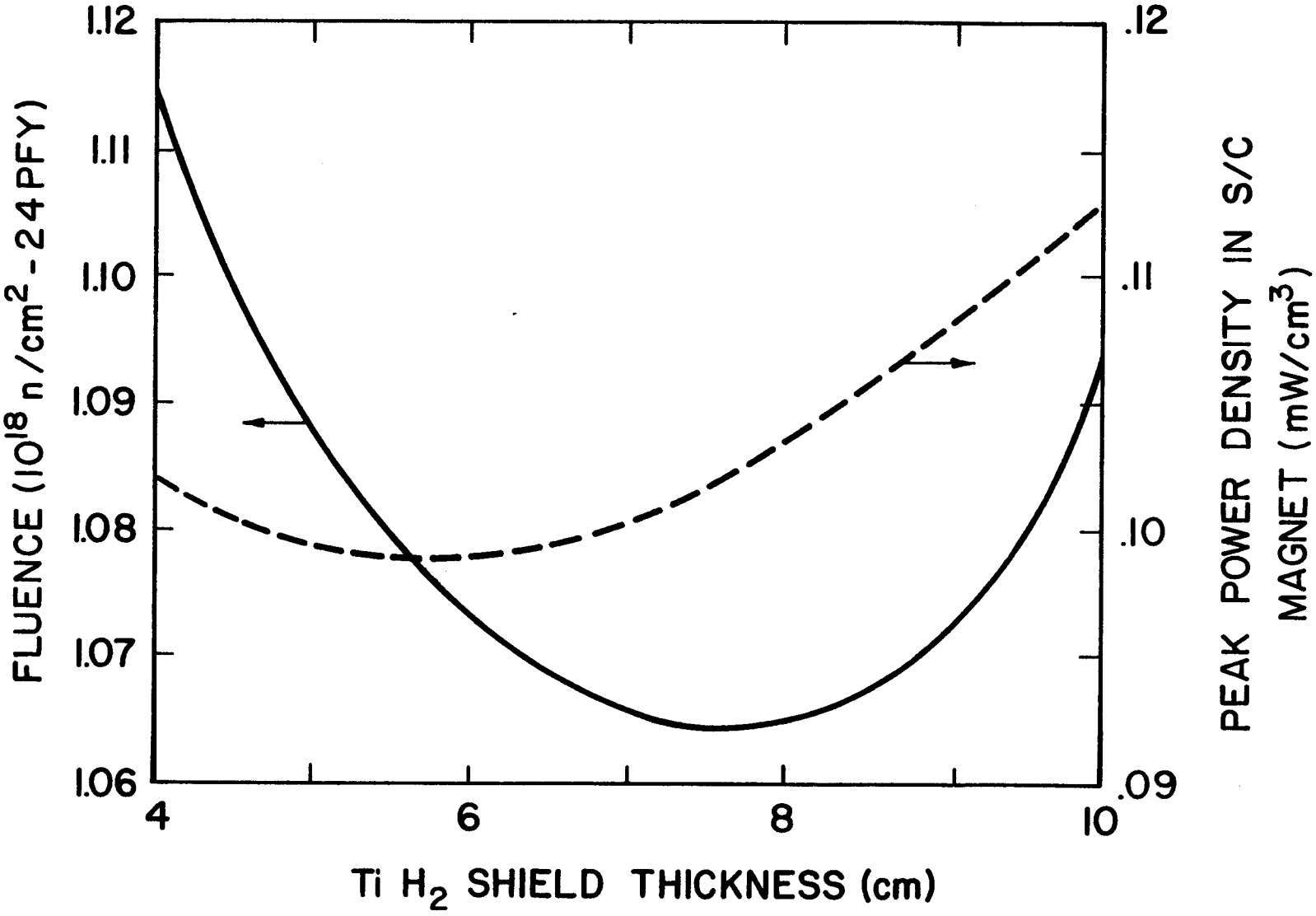

Fig. 3-2. Effect of adding TiH_2-shield at the back of 0.8 m W-shield.

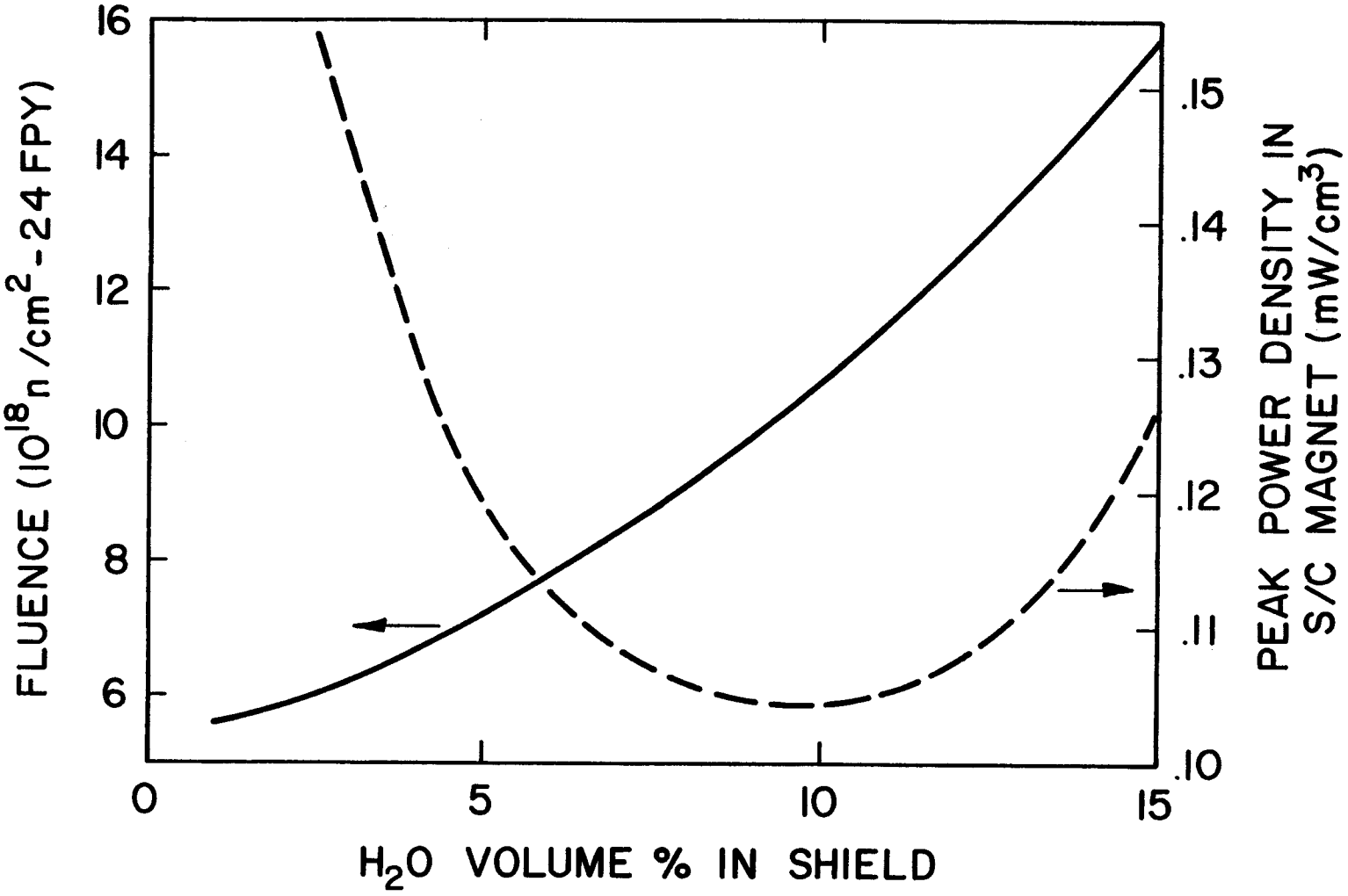

Fig. 3-3. Effect of varying the water content in a 0.8 m thick W and TiH_2-shield.

Fig. 3-4. Effect of adding boric acid in the cooling water of the shield.

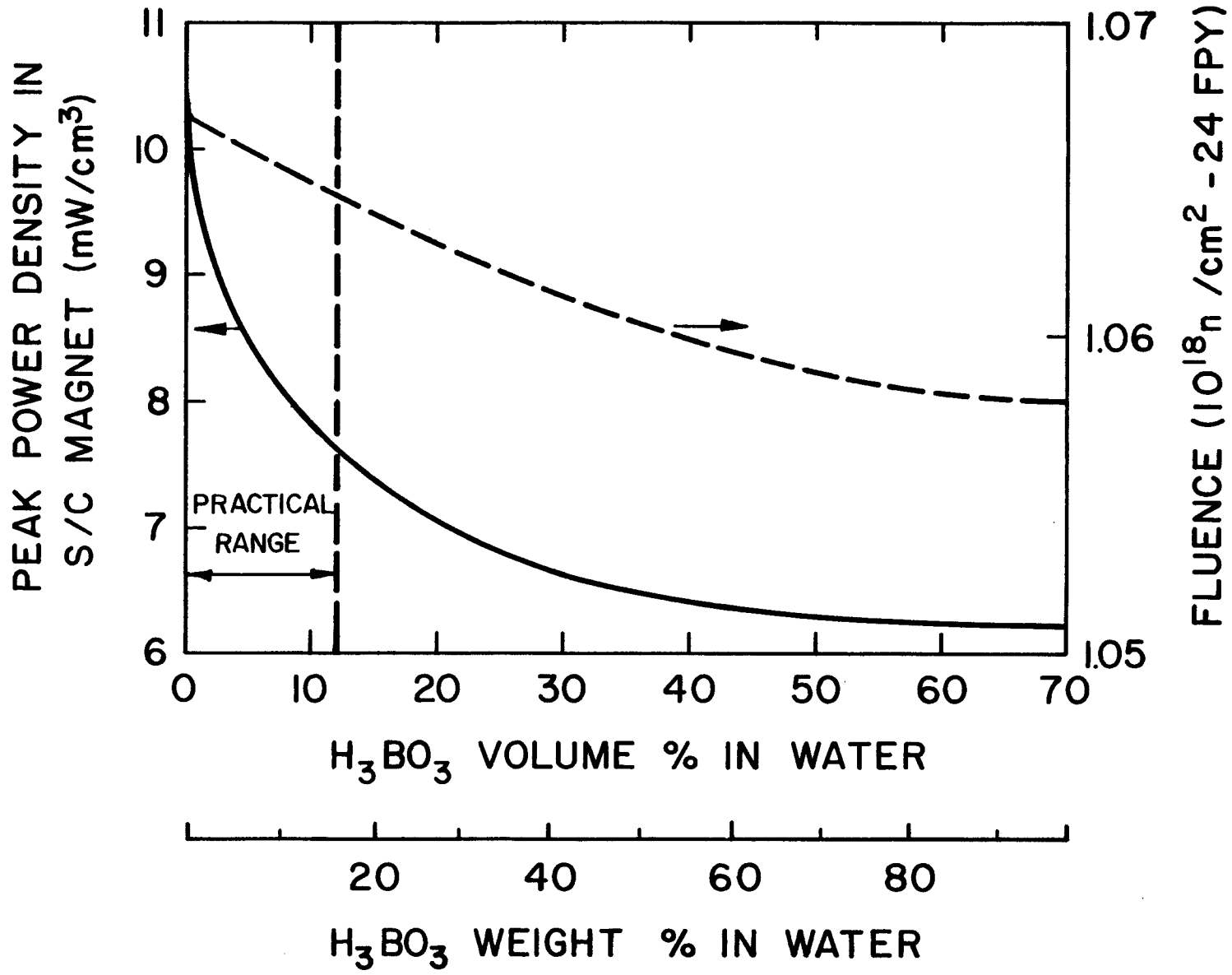

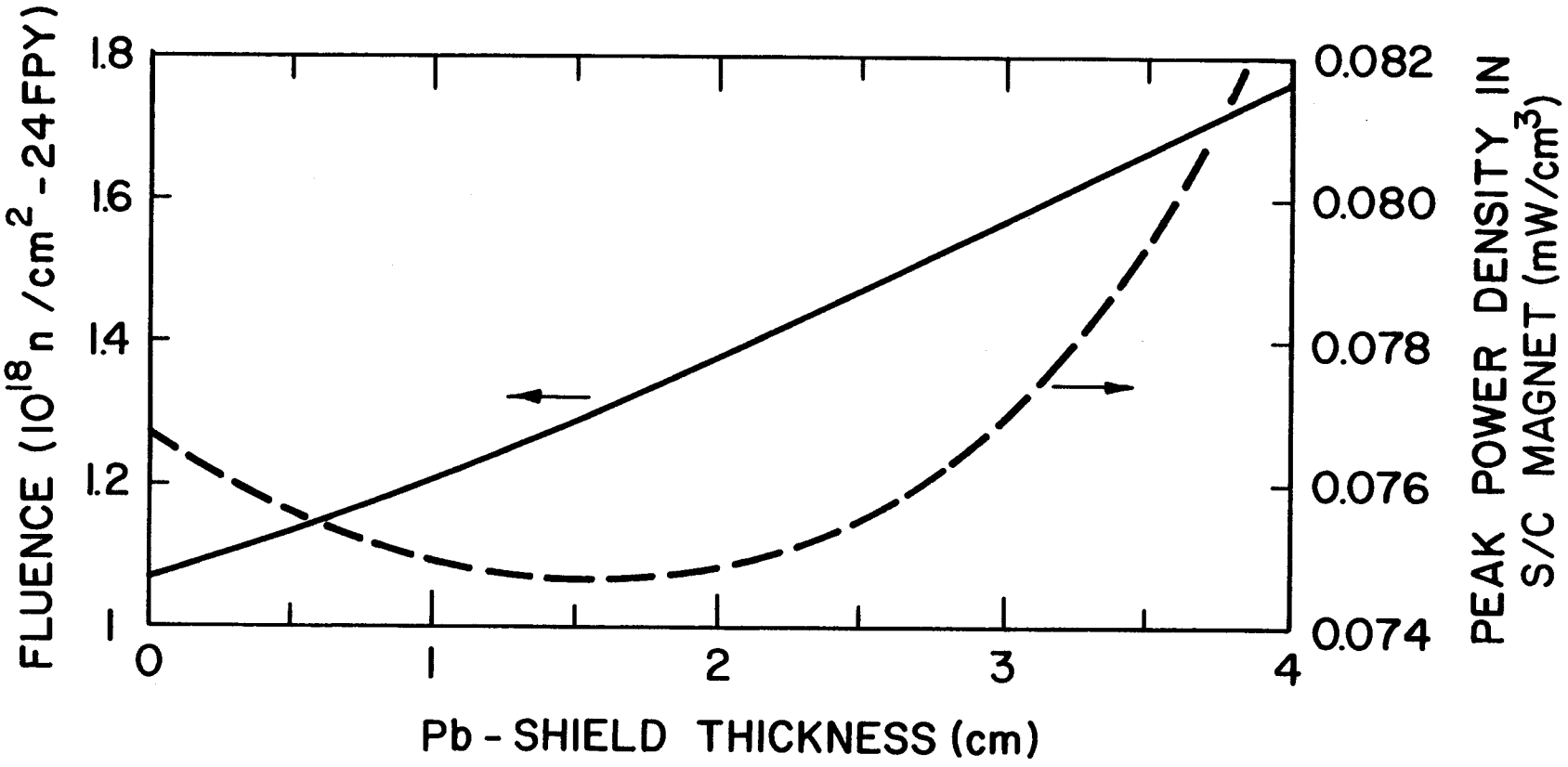

Fig. 3-5. Effect of backing the W and TiH_2-shield by Pb-shield.

magnet through the attenuation of the gamma rays. However, it is not particularly helpful in reducing the fast neutron fluence, as expected. The effect of the B_4C-shield (80 vol.% B_4C [90% ^{10}B in B], 10 vol.% Fe-1422, and 10 vol.% H_2O) was also examined in a 0.8 m thick W-shield. Figure 3-6 reveals that 0.07 m of B_4C-shield is required at the coil side of the W-shield to minimize the fast neutron fluence. However, our results (see Fig. 5-2) show that a ~ 56% greater reduction was achieved in case of backing the W-shield by a 0.08 m TiH_2-shield. In conclusion, a shield consisting of W and TiH_2 arranged as described above has proven to be the most effective shield in reducing the fast neutron fluence.

The 0.8 m thick W and TiH_2 optimal shield actually provided more shielding than the design goals. The effect the shield thickness has on the radiation effects in the S/C magnet is provided in Fig. 3-7. The fast neutron fluence limit of 4×10^{19} n/cm^2 per 24 FPY dictated the choice of a 0.6 m thick inboard shield to protect the S/C magnet. Other corresponding data of interest are the peak power density in the S/C magnet, peak dpa rate in the Cu stabilizer, and the peak dose in the GFF polyimide insulator. These are 2.2 mW/cm^3, 1.2×10^{-3} dpa/FPY, and 7.4×10^{10} rad/24 FPY, respectively.

One other interesting result is the shield thickness required for different neutron wall loadings. It is worth mentioning that decreasing the wall loading by a factor of 2 will only thin the shield by ~ 4 cm, as shown in Fig. 3-8.

3.2 Neutron Wall Loading Distribution

Special effort was devoted to calculating the neutron wall loading distribution in the poloidal direction. This poloidal variation was of concern in many tokamak reactor studies,[3,4] and the problem stems from the fact that

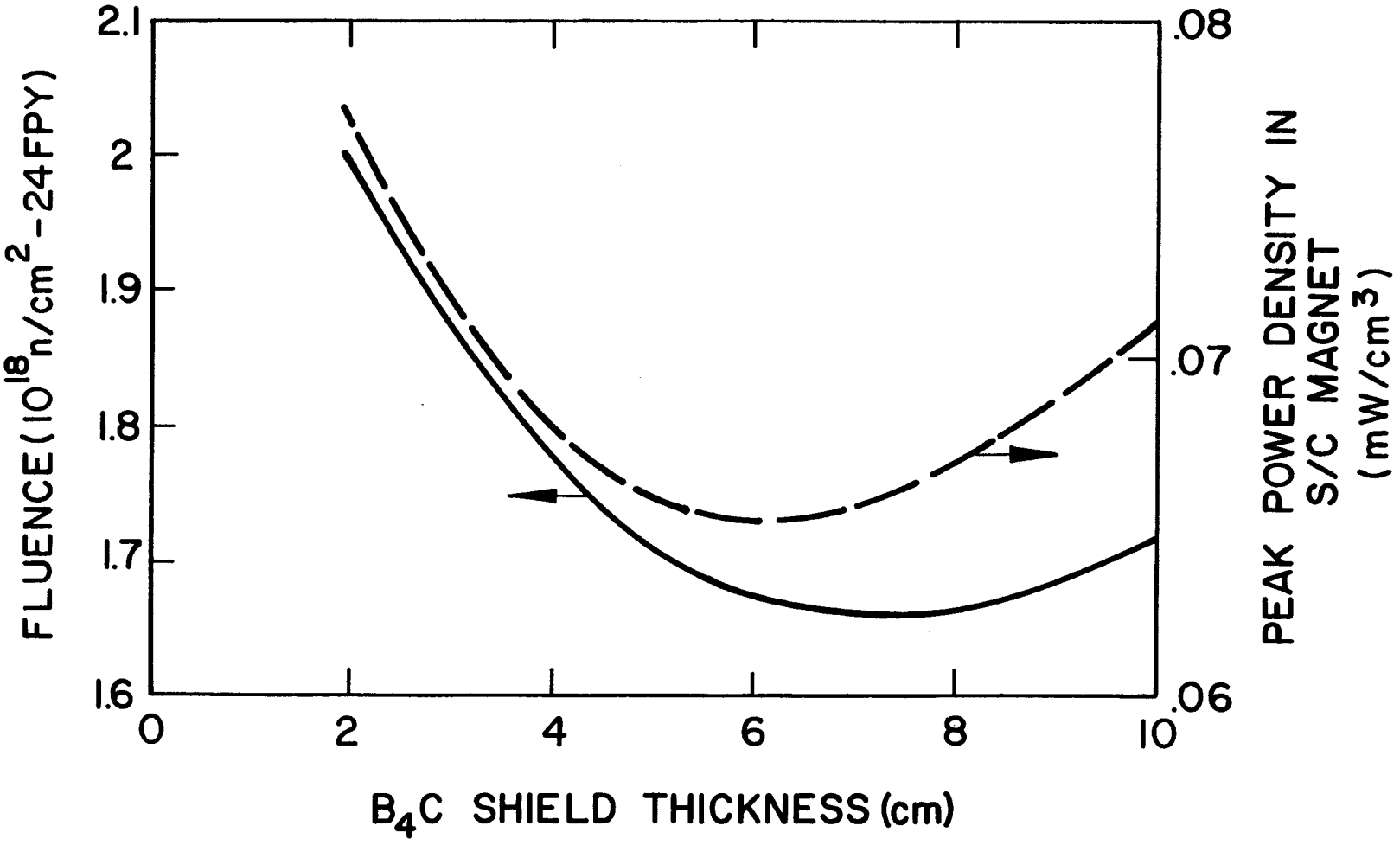

Fig. 3-6. Effect of backing the W-shield by B_4C-shield.

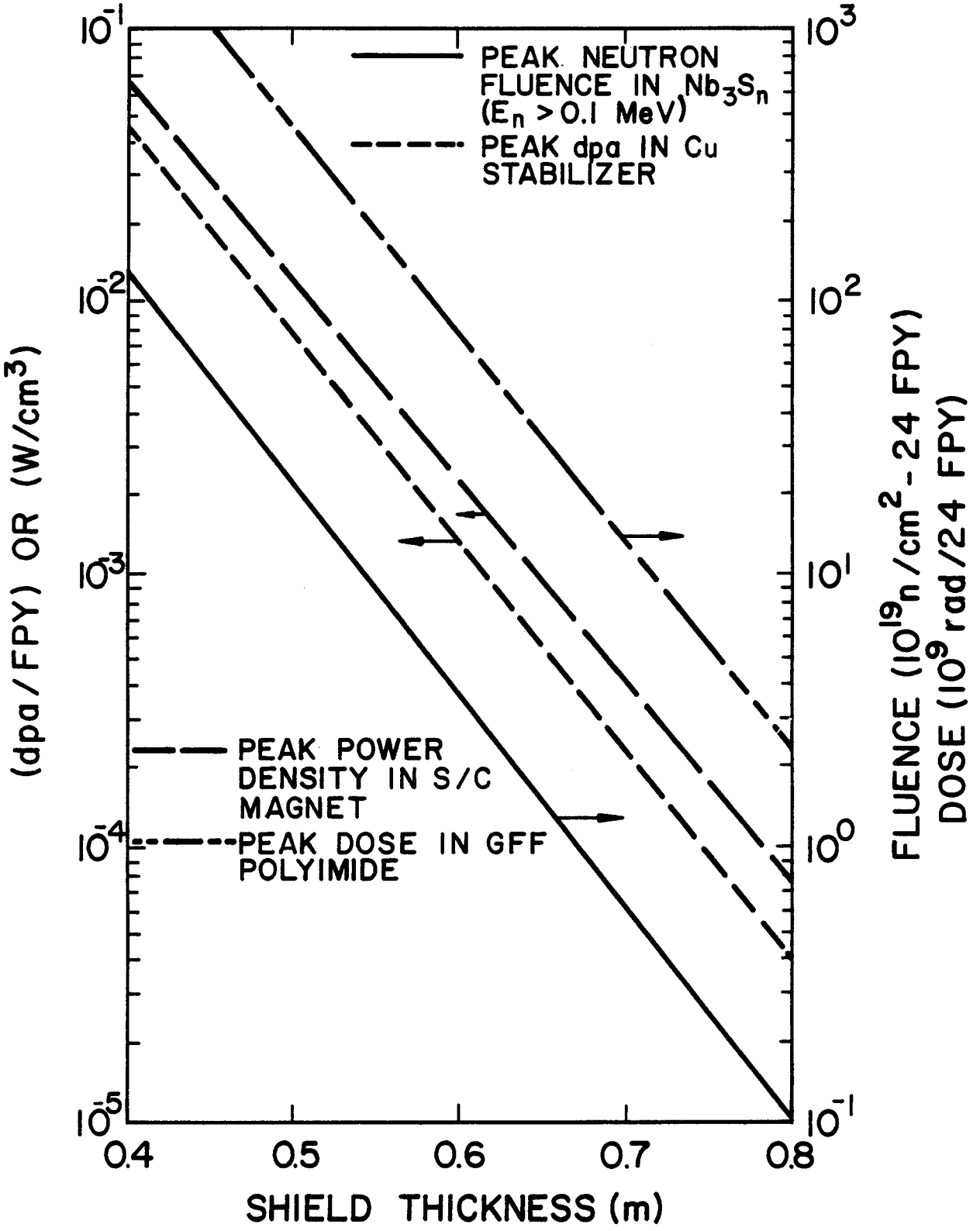

Fig. 3-7. Variation of the radiation effects in the S/C magnet with the inboard shield thickness for 10 MW/m² wall loading.

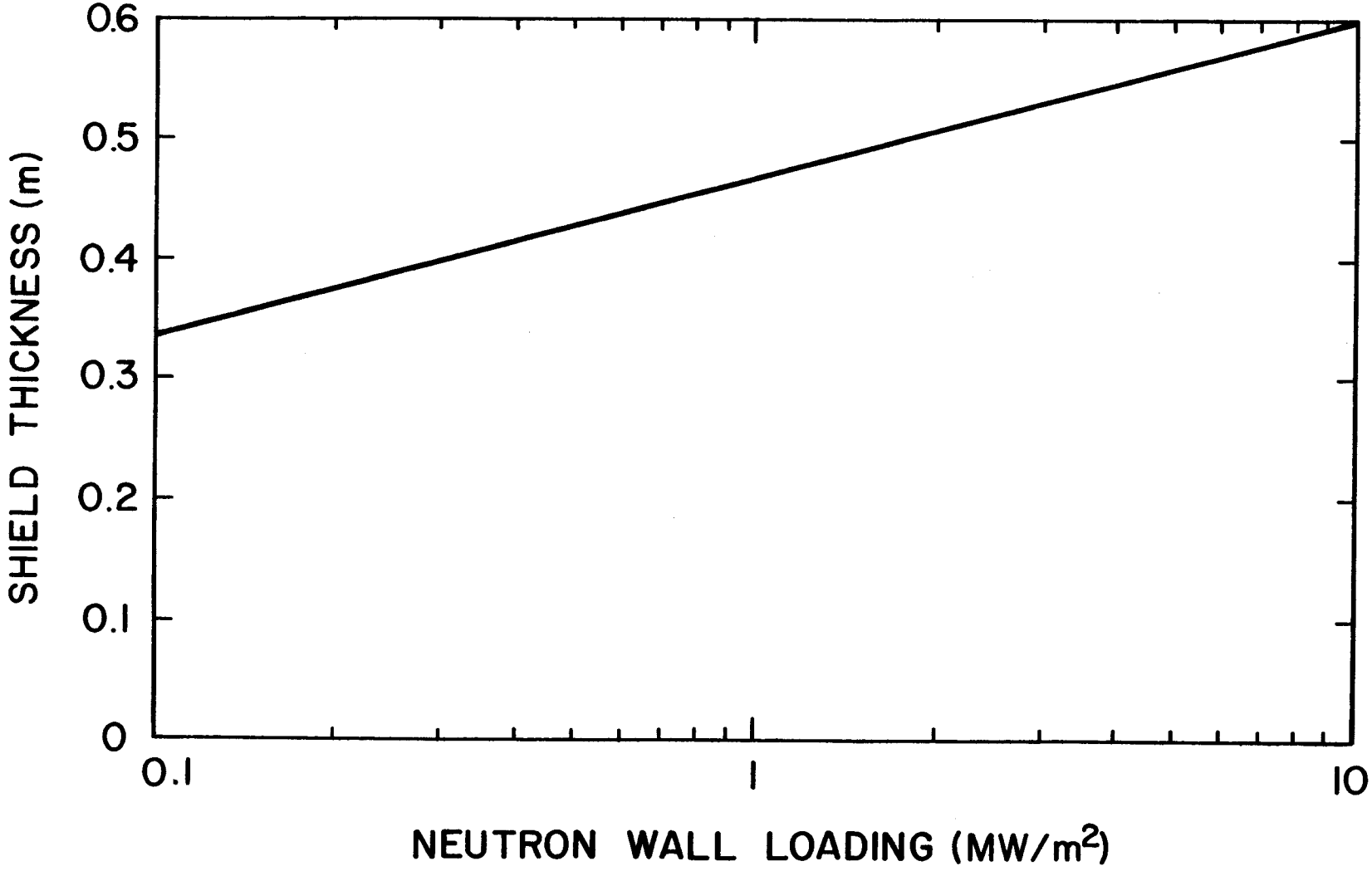

Fig. 3-8. The required inboard shield thickness for different wall loadings.

the peak neutron wall loading is located off-axis. This depends on several factors: the aspect ratio of the reactor, the shape of the plasma boundary and first wall, and the spatial distribution of the plasma density within the plasma boundary.

The preliminary reactor design was modeled for the three-dimensional Monte Carlo code MCNP.[5] The model was for major and minor radii of 3.07 and 0.55 m, respectively, and a fusion power of 1150 MW. Due to symmetry, only one-eighth of the reactor geometry was modeled and several reflecting boundaries were appropriately located, as indicated in Fig. 3-9. The simple case of uniform plasma density was considered and trapping surfaces were located at the first wall to count all crossing neutrons. A run of 10,000 histories yields the neutron wall loading distribution given in Fig. 3-10 and the statistical uncertainty is less than 2%. The distribution is characterized by two off-axis peaks: one (9.04 MW/m^2) at the inboard shield and the other (10.16 MW/m^2) at the outboard blanket. The average wall loading is 9.33 MW/m^2. As a major goal of this study is to provide an inboard neutron wall loading of 10 MW/m^2, the system code will be used to design the reactor such that the peak neutron wall loading of 10 MW/m^2 is achieved at the inboard surface. This will require a wall loading of ~ 11 MW/m^2 at the plasma boundary, as explained in Chapter 4.

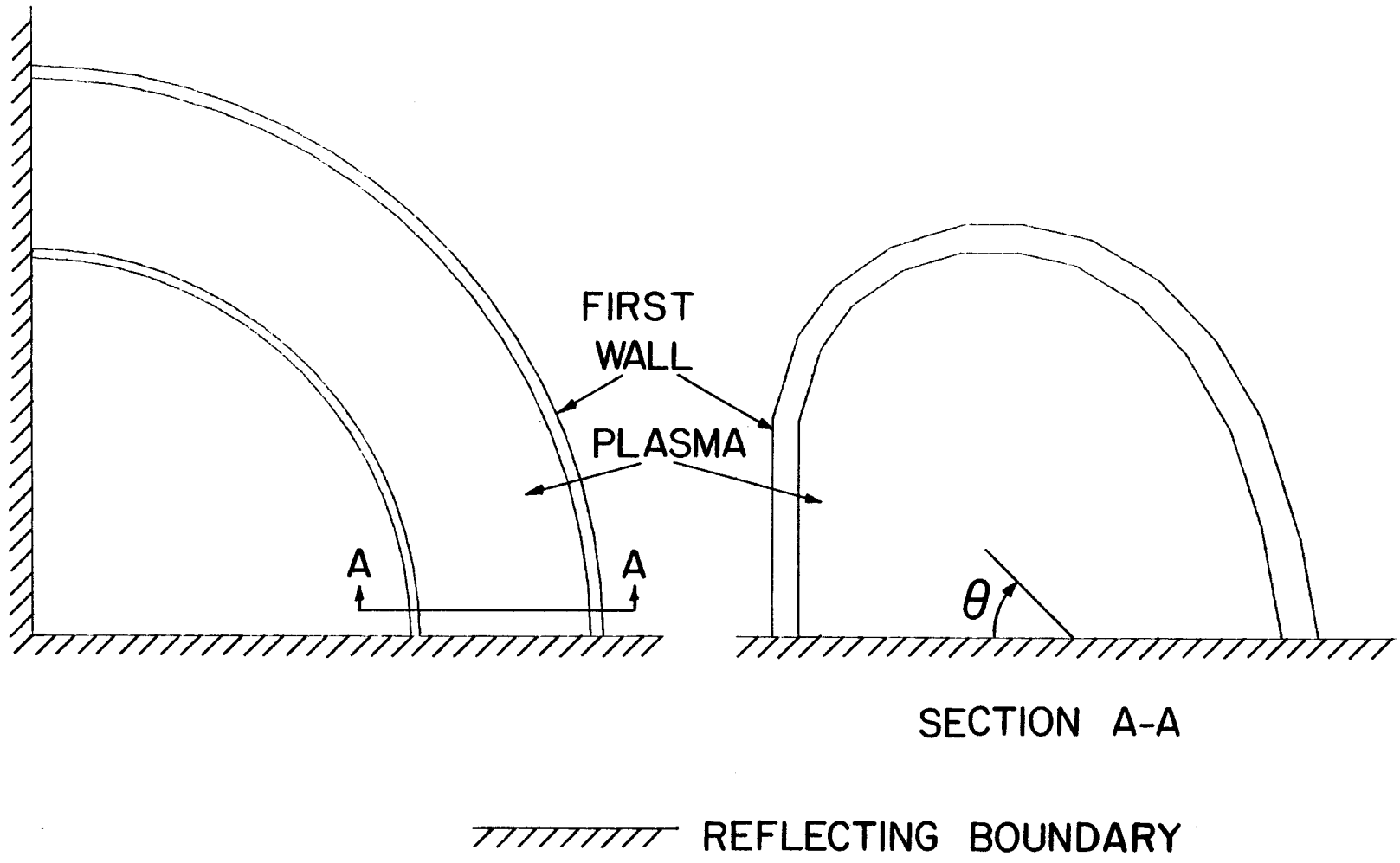

CALCULATIONAL MODEL FOR THE NEUTRON WALL LOADING DISTRIBUTION

Fig. 3-9. The geometrical model used for the three-dimensional calculations of the neutron wall loading distribution.

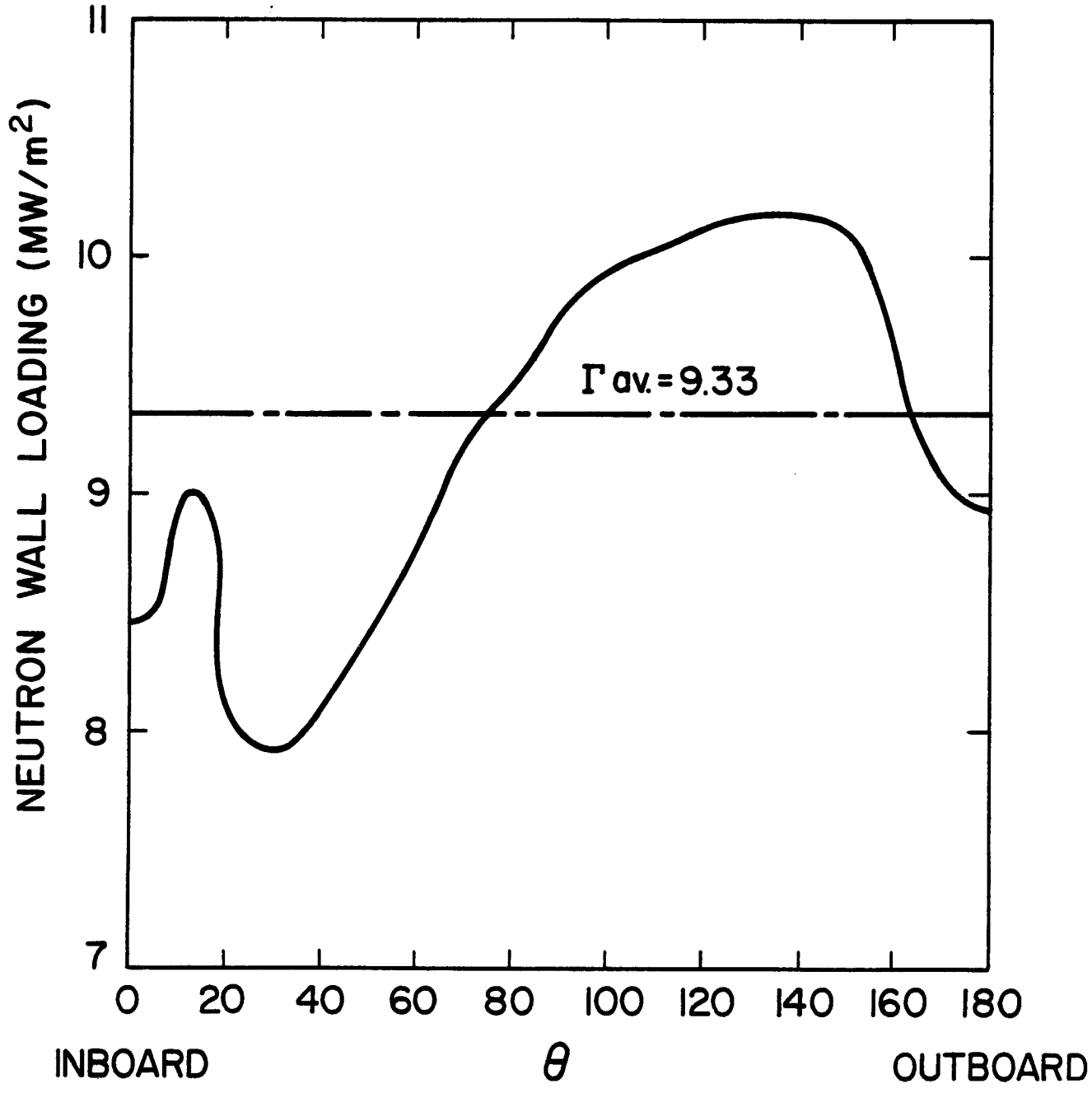

Fig. 3-10. The poloidal variation of the neutron wall loading for the preliminary reactor design.

References for Chapter 3

1. R.D. O'Dell et al., "User's Manual for ONEDANT: A Code Package for One-Dimensional, Diffusion-Accelerated, Neutral Particle Transport," LA-9184-M, Los Alamos National Laboratory (Feb. 1982).

2. Von Stackelberg et al., Electrochem. 43, 21 (1937).

3. B. Badger et al., "UWMAK-III - A Noncircular Tokamak Power Reactor Design," University of Wisconsin Fusion Engineering Program Report UWFDM-150 (1976).

4. C.C. Baker et al., "STARFIRE - A Commercial Tokamak Fusion Power Plant Study," ANL/FPP-80-1, Fusion Power Program, Argonne National Laboratory (1980).

5. Los Alamos National Laboratory Group X-6, "MCNP - A General Monte Carlo Code for Neutron and Photon Transport, Version 2D," LA-7397-M, Revised, Los Alamos National Laboratory (April 1981).

4. General System Parameters

4.1 Introduction

This chapter summarizes the general system parameters that were chosen and calculated for the device. The choice of some of these parameters is based on the results and the conclusions of previous reactor designs. However, the selection of the major parameters (e.g. aspect ratio Ar, plasma radius A, wall loading Γ_w , fusion power P_f, beta (β), maximum field at the magnet B_{max}) is based on extensive parameter survey that was made by the use of the Tokamak Systems Code (TSC).

4.2 Tokamak Systems Code (TSC)

The TSC was developed at the FEDC. Up to the present no documentation is available for this code that describes the mathematical and theoretical models adopted in the different modules of the code. As it stands now, the TSC, Version 2, has many modules to calculate the various subsystem parameters, and requires numerous input parameters. Figure 4-1 shows a flow chart of the code. In this study we have used only three modules (Fig. 4-2), the physics module, the first wall/shielding module, and the toroidal magnet module. The physics module was modified such that it iterates on the field at the plasma center to obtain the required neutron loading. The magnet module was also modified to iterate on the aspect ratio to obtain the aspect ratio that corresponds to the specific input value of the field at the magnet (B_{max}). Generally the first wall/shielding module was used just to establish the geometrical relations required by the magnet module. All the neutronic calculations were done externally, as shown in the previous and the following chapters.

TOKAMAK SYSTEMS CODE FLOW DIAGRAM

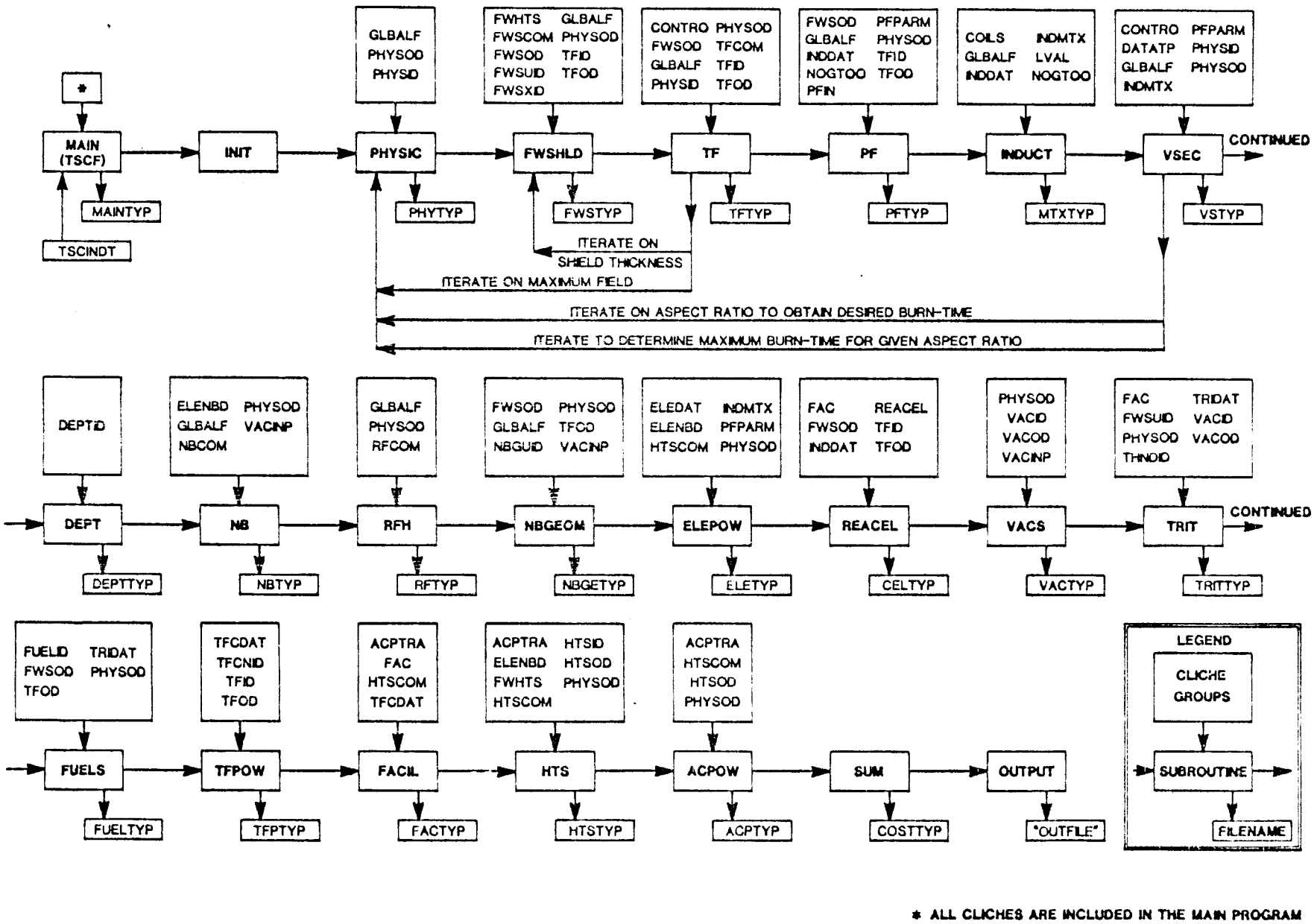

Fig. 4-1. Flow chart of the TSC.

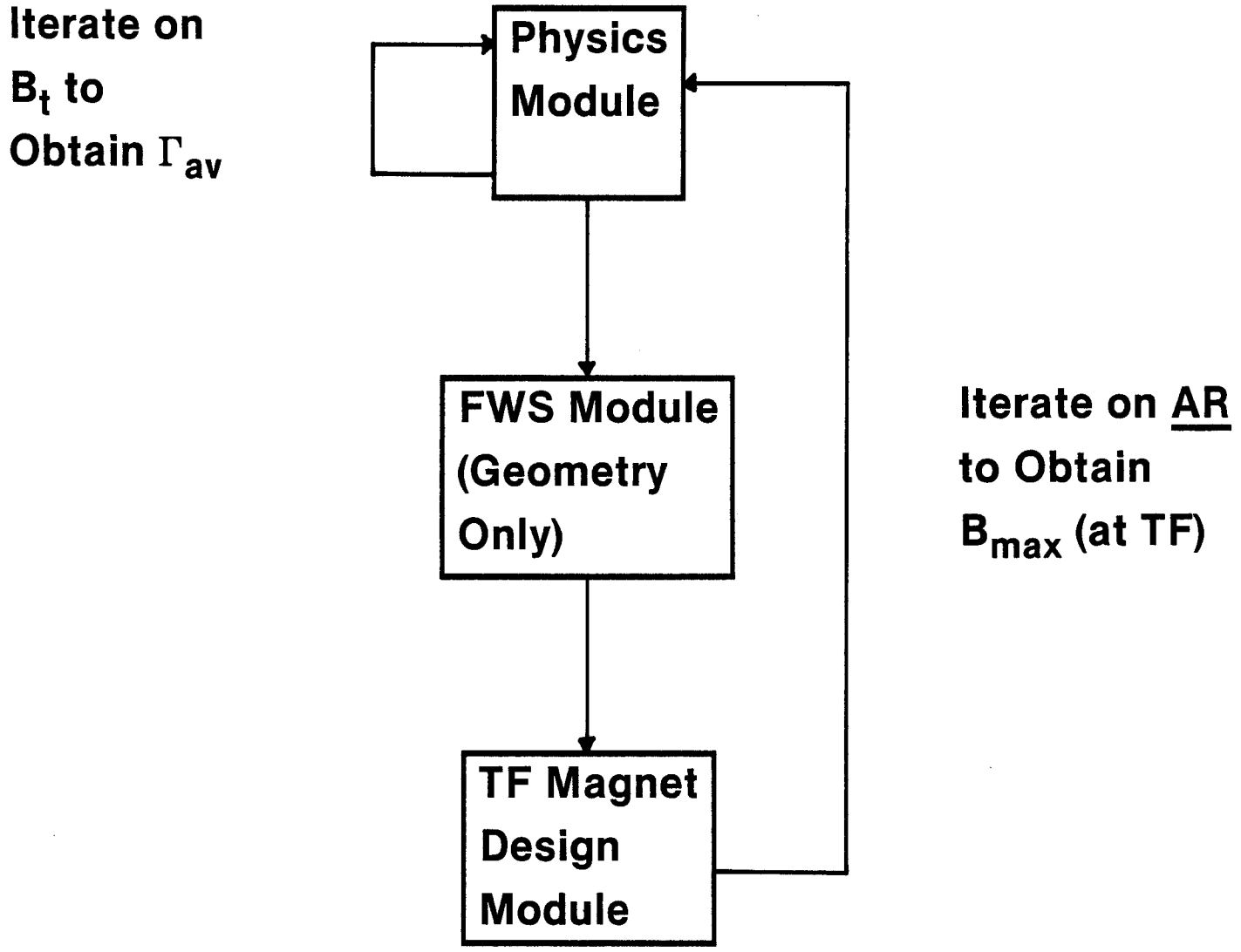

Fig. 4-2. Modified TSC.

4.3 Constraints and Assumptions

A. Maximum Field at the TF Magnets. Using Nb_3Sn, the maximum field at the TF magnets is limited to 16 T. This limit could be relaxed by using a hybrid coil to obtain the same field at the plasma center for the same neutron loading, but as it turned out, the required power for the copper coil is unacceptable (Chapter 7).

B. TF Current Density. We used an average value for the current density of 4000 A/cm^2 over the winding pack of the TF magnet. However, the change of this current density affects only the cross section of the magnet and as long as no inductive action was assumed to be required to induce or to maintain the plasma current, the value of the current density is not crucial (see Figs. 4-11a and 4-11b).

C. Transformer Action. No transformer action was assumed to be required either to induce the plasma current or to maintain it. This assumption removes an important constraint on the required size of the inner core of the device. It should be mentioned here that, for long burn times ($> 10^4$ s), to sustain the plasma current inductively is more demanding on the size of the inner core than to initiate this current inductively.

D. Thermal Power. We set, at the beginning, a limit of 1000 MW for the fusion power. But it turned out that, for reasonable values of the aspect ratio, this limit is impossible to reach unless higher and more aggressive values of beta ($\beta_t \sim 10\%$) are used.

E. Neutron Loading. The TSC produces only an average value of the neutron loading at the plasma edge. To obtain a peak neutron wall loading of 10 MW/m^2 at the inboard first wall, several average values of the plasma edge average neutron loading (10, 11 and 12 MW/m^2) were considered and itera-

tive neutronic calculations, taking into account the change of the fusion power and the aspect ratio, were performed (see Fig. 4-6 to Fig. 4-8).

F. Fixed Plasma Input Parameters. Table 4-1 shows some of the plasma parameters that were chosen for this study. The selection of these parameters was based on the results and conclusions of previous conceptual reactor designs. No attempt has been made here to vary these parameters which could modify our results.

G. Inboard Dimensions. The dimensions from the left edge of the plasma to the inboard winding pack of the magnet are selected as follows: 6 cm scrapeoff, 1 cm first wall thickness, 60 cm shield thickness, 3 cm gap, and 17 cm for the cryostat walls, dewar, insulation, etc. Thus a total of 87 cm thickness is assumed from the plasma edge to the inboard winding pack. The thickness of the shield (60 cm) was chosen according to the neutronic calculations in Chapter 3.

Table 4-1. Fixed Plasma Input Parameters

Elongation	1.6
Triangularity	.3
Safety Factor	2.0
Electron temperature (keV)	13
Ion temperature (keV)	13
Z_{eff}	1.5
Z_{imp}	8

4.4 Results and Discussion

A wide range of plasma radii, aspect ratios, and maximum fields was used in the parameteric survey. The plasma radii range from 35 cm to 70 cm. The aspect ratios range is from 4 to 12, and this corresponds to a major radius range of 300 to 420 cm. The maximum field values considered ranged from 10 T to 16 T. Three values of the average neutron loading at the plasma boundary are used, and these are 10, 11 and 12 MW/m^2.

Two values of beta (β) are considered, namely 6% and 8%. To show the major effect of this crucial parameter, a more aggressive value of β = 10% is also considered. The value of β = 8% is our base value.

Figures 4-3 to 4-5 show the variation of the maximum field at the TF magnet for 10, 11 and 12 MW/m^2 average neutron wall loding Γ_{av}. The effect of increasing Γ_{av} is to increase the required field for the same aspect ratio and the same plasma radius. For the same field and the same plasma radius, an increase in wall loading increases the required aspect ratio.

The fusion power as a function of the aspect ratio and for different minor radii is shown in Figs. 4-6 to 4-8 for the different wall loading. The lowest fusion power for each plasma radius in these figures corresponds to a maximum field of 16 T at the TF magnet. It is clear in comparing these figures that the increase in the fusion power due to the increase in Γ_{av} is accompanied by an increase in the aspect ratio for the same B_{max}, or higher B_{max} for the same aspect ratio.

The effect of β, for the same neutron loading Γ_{av} = 11 MW/m^2, on the fusion power and the aspect ratio can be shown by comparing Fig. 4-8, 4-9, and 4-10, which are for β = 8%, β = 6% and β = 10% respectively. Two interesting points can be made in this comparison. First, increasing beta will decrease

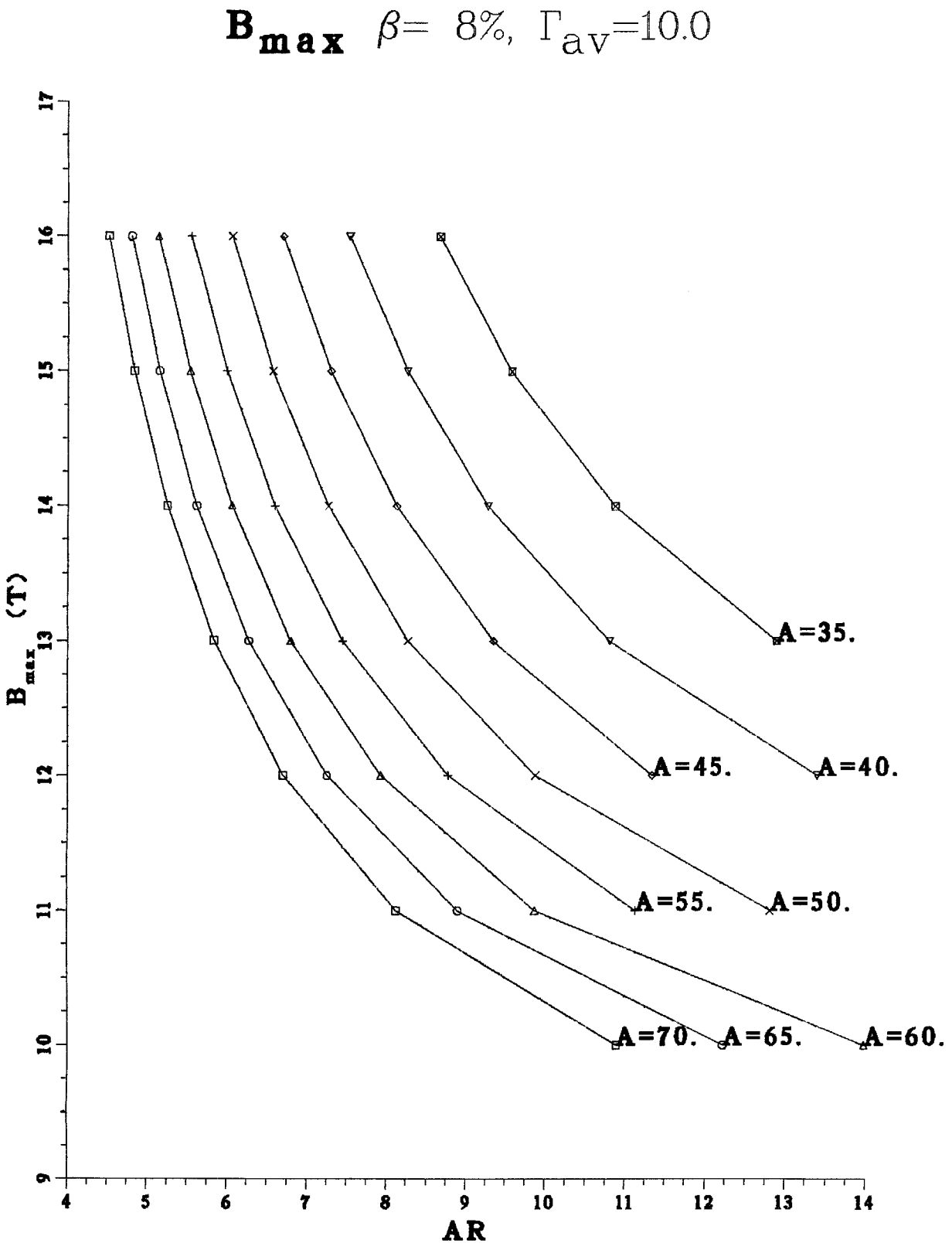

Fig. 4-3. B_{max} versus aspect ratio for Γ_{av} = 10 MW/m^2.

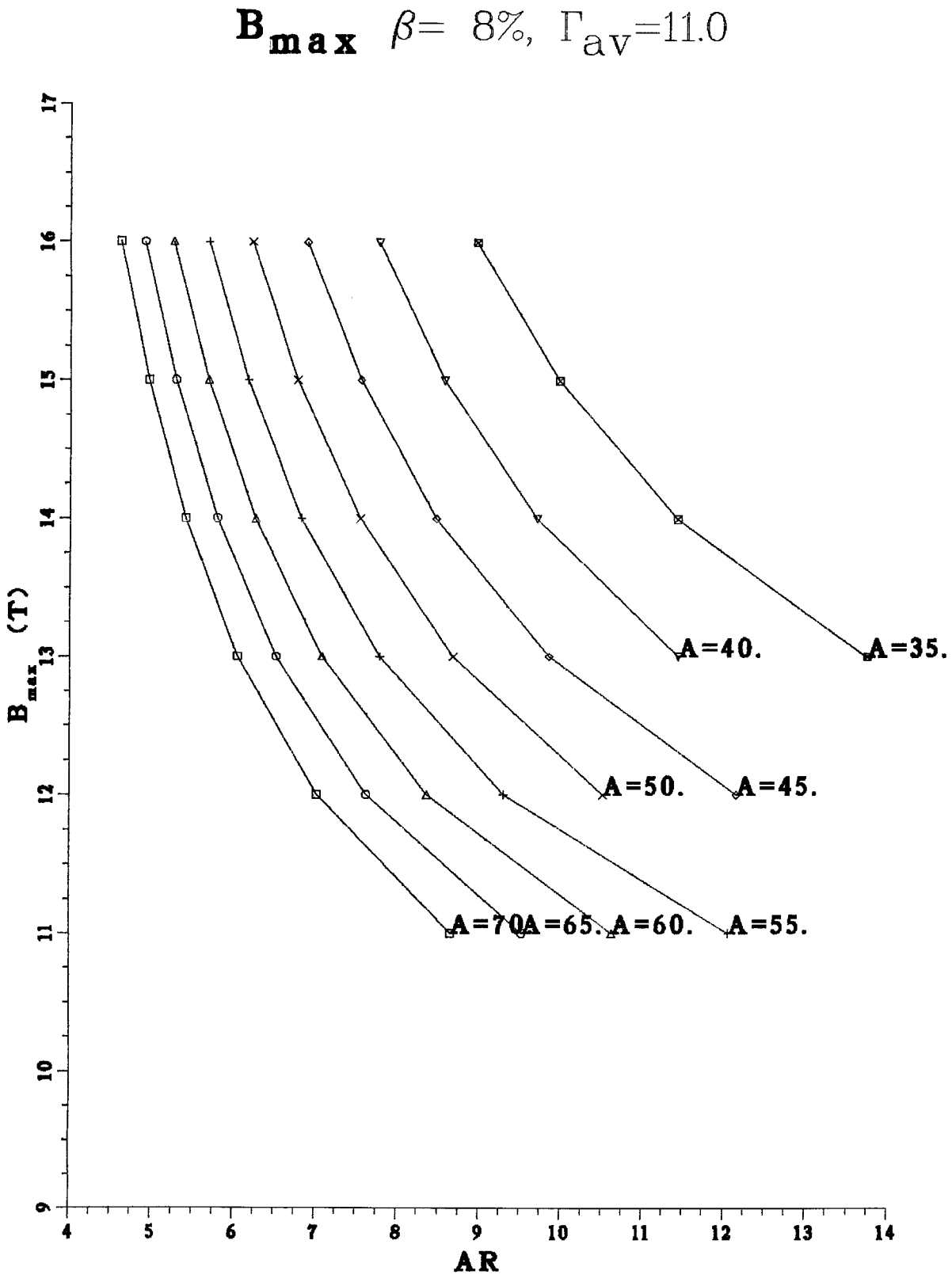

Fig. 4-4. B_{max} versus aspect ratio for Γ_{av} = 11 MW/m^2.

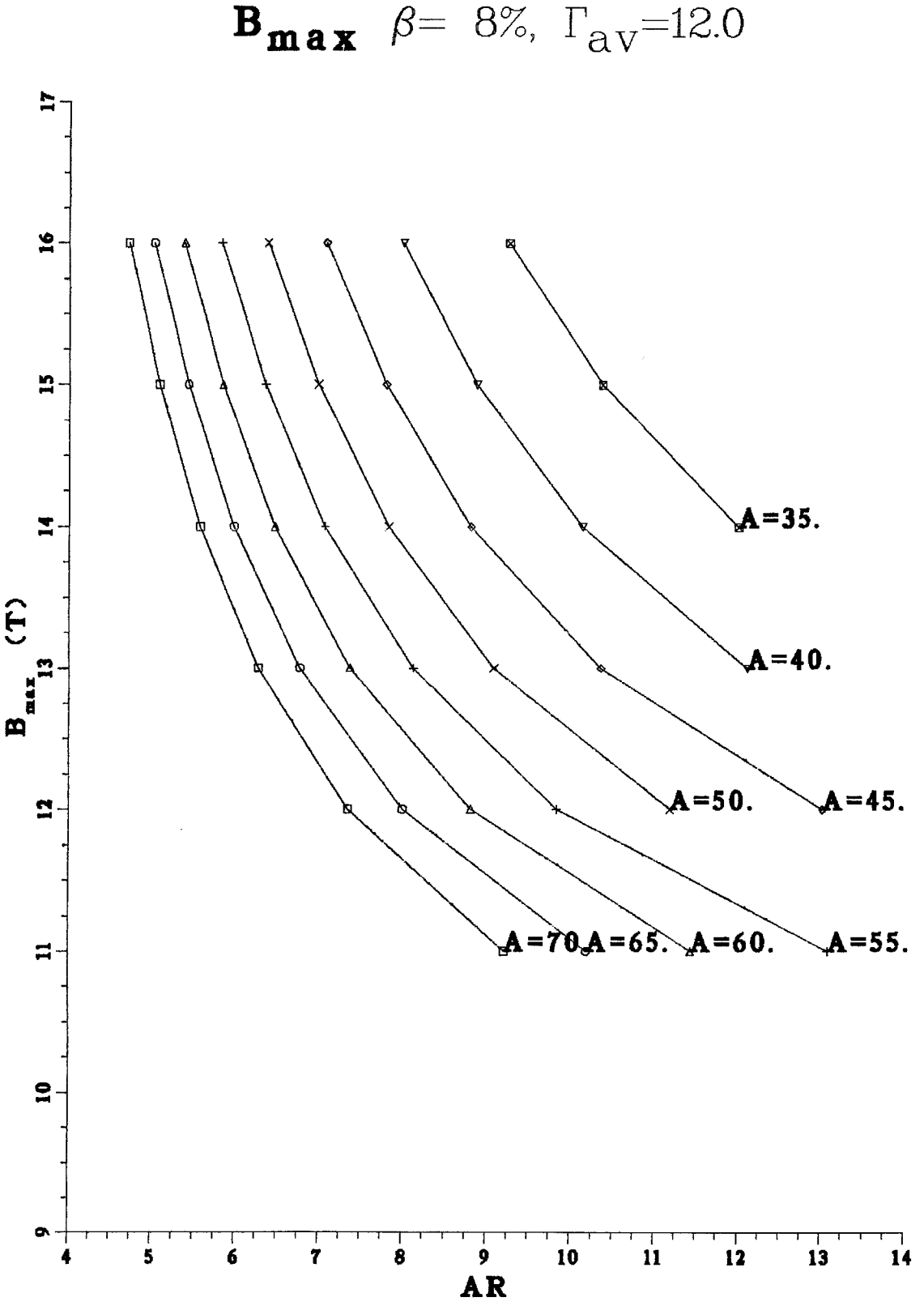

Fig. 4-5. B_{max} versus aspect ratio for Γ_{av} = 12 MW/m^2.

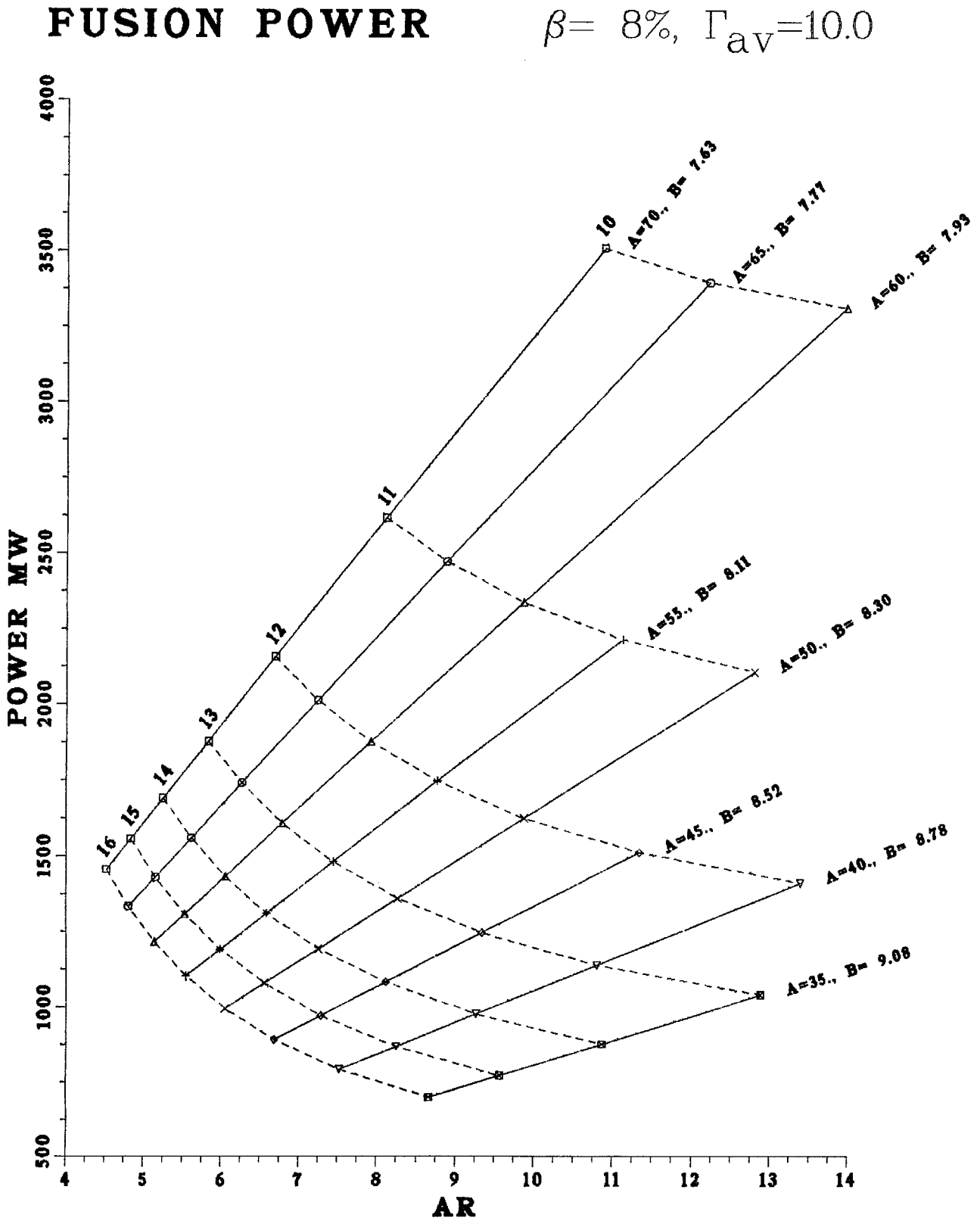

Fig. 4-6. P_f versus aspect ratio for Γ = 10 MW/m^2.

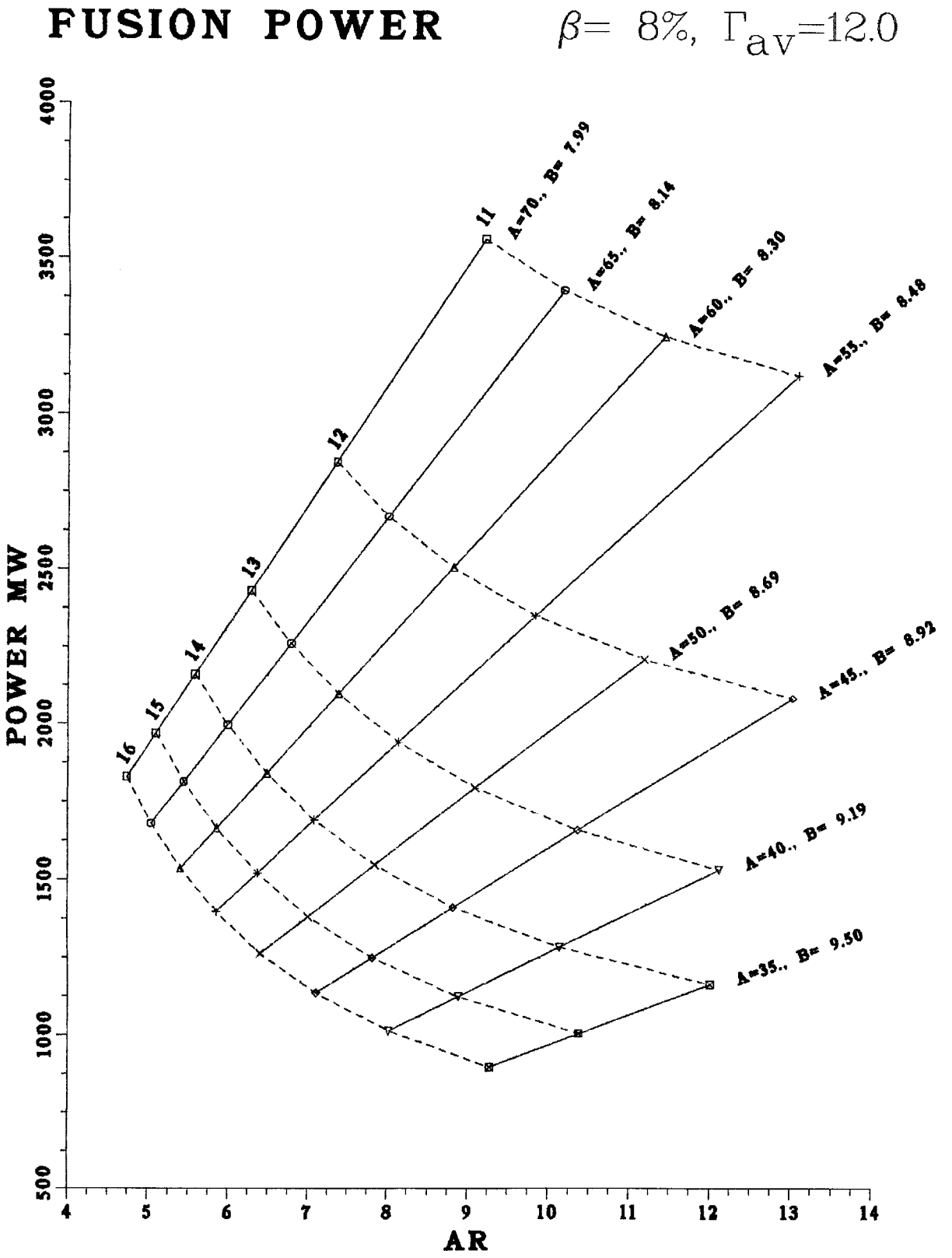

Fig. 4-7. P_f versus aspect ratio for Γ = 12 MW/m^2.

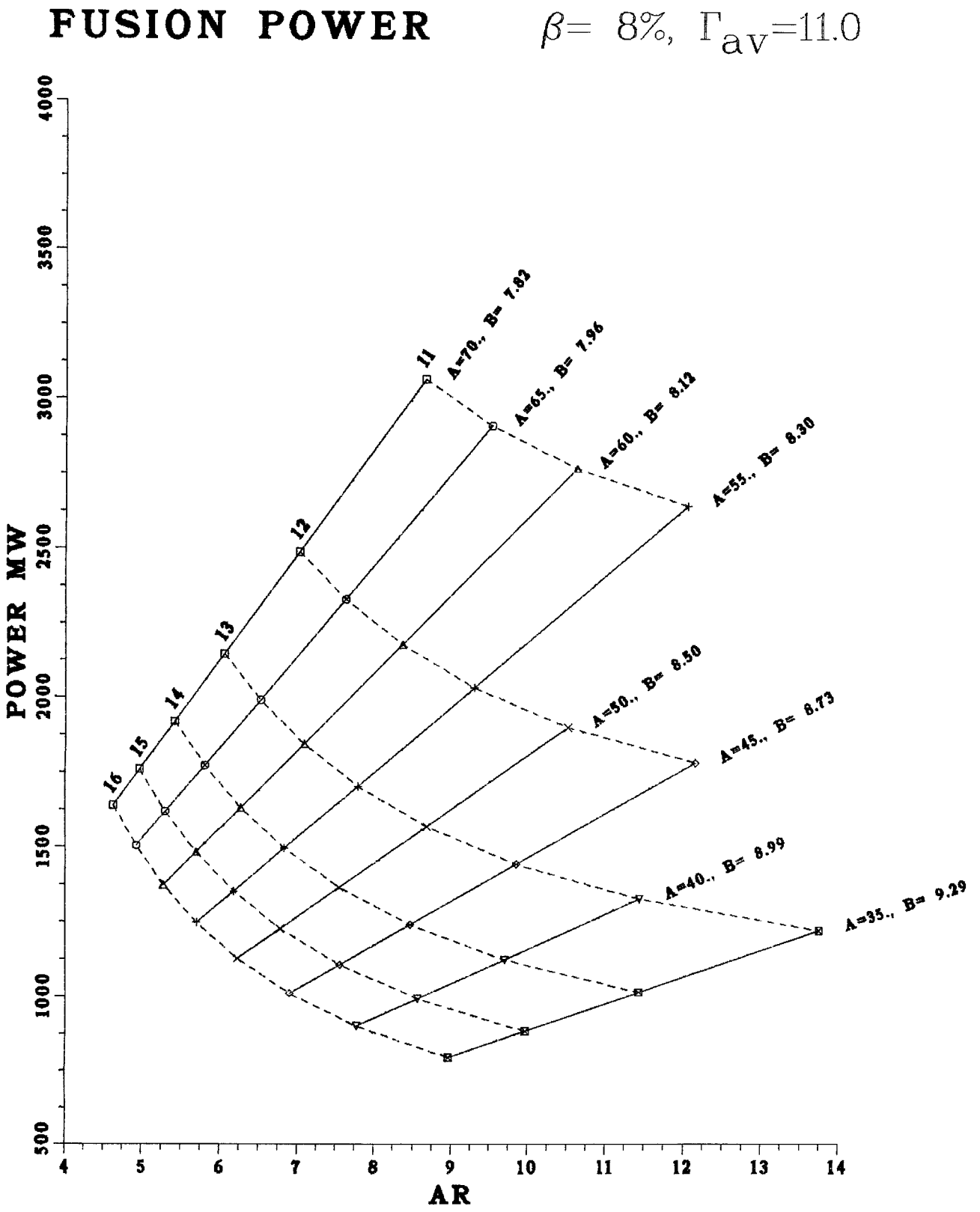

Fig. 4-8. P_f versus aspect ratio for Γ = 11 MW/m^2.

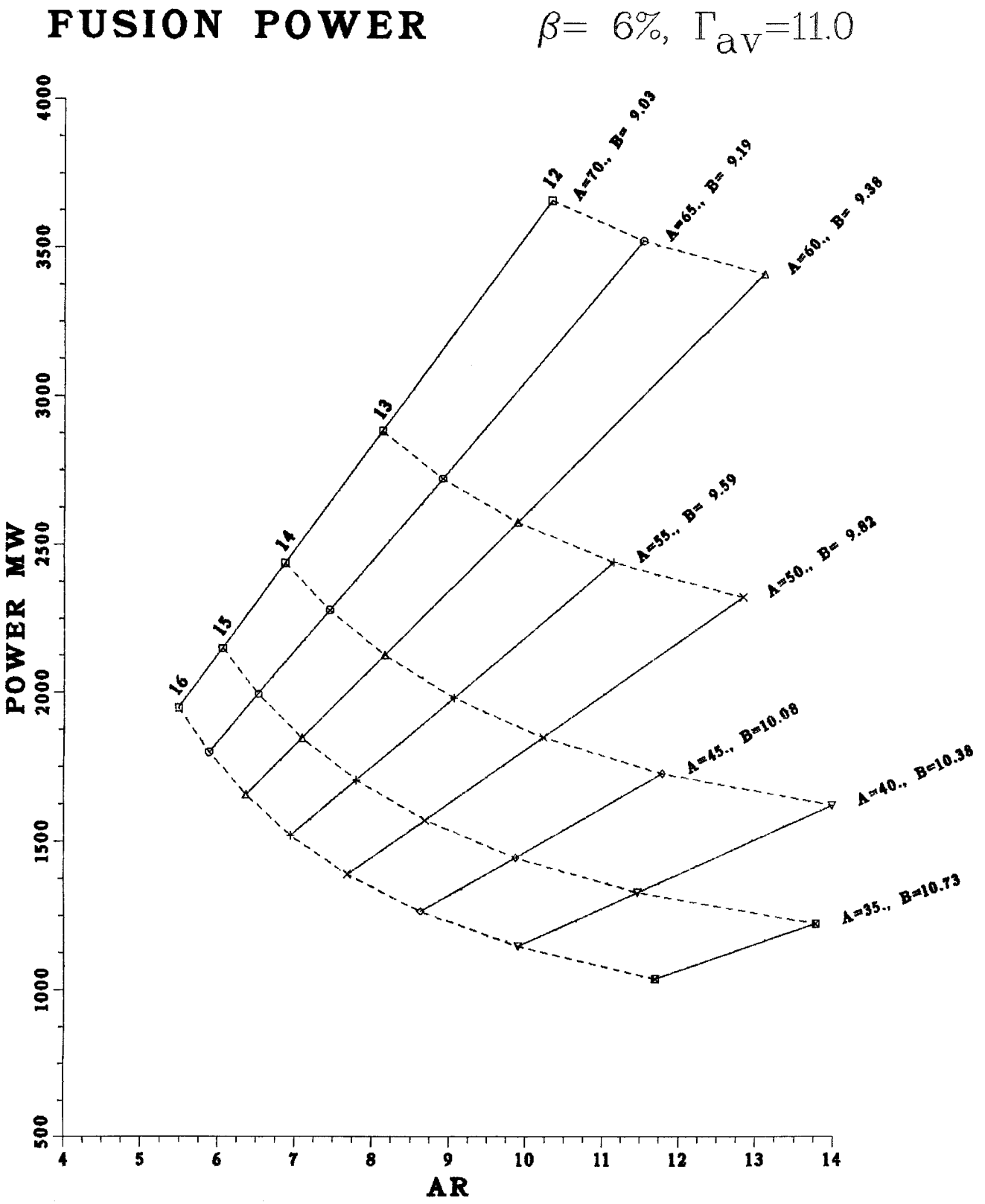

Fig. 4-9. P_f versus aspect ratio for Γ = 11 MW/m^2, β = 6%.

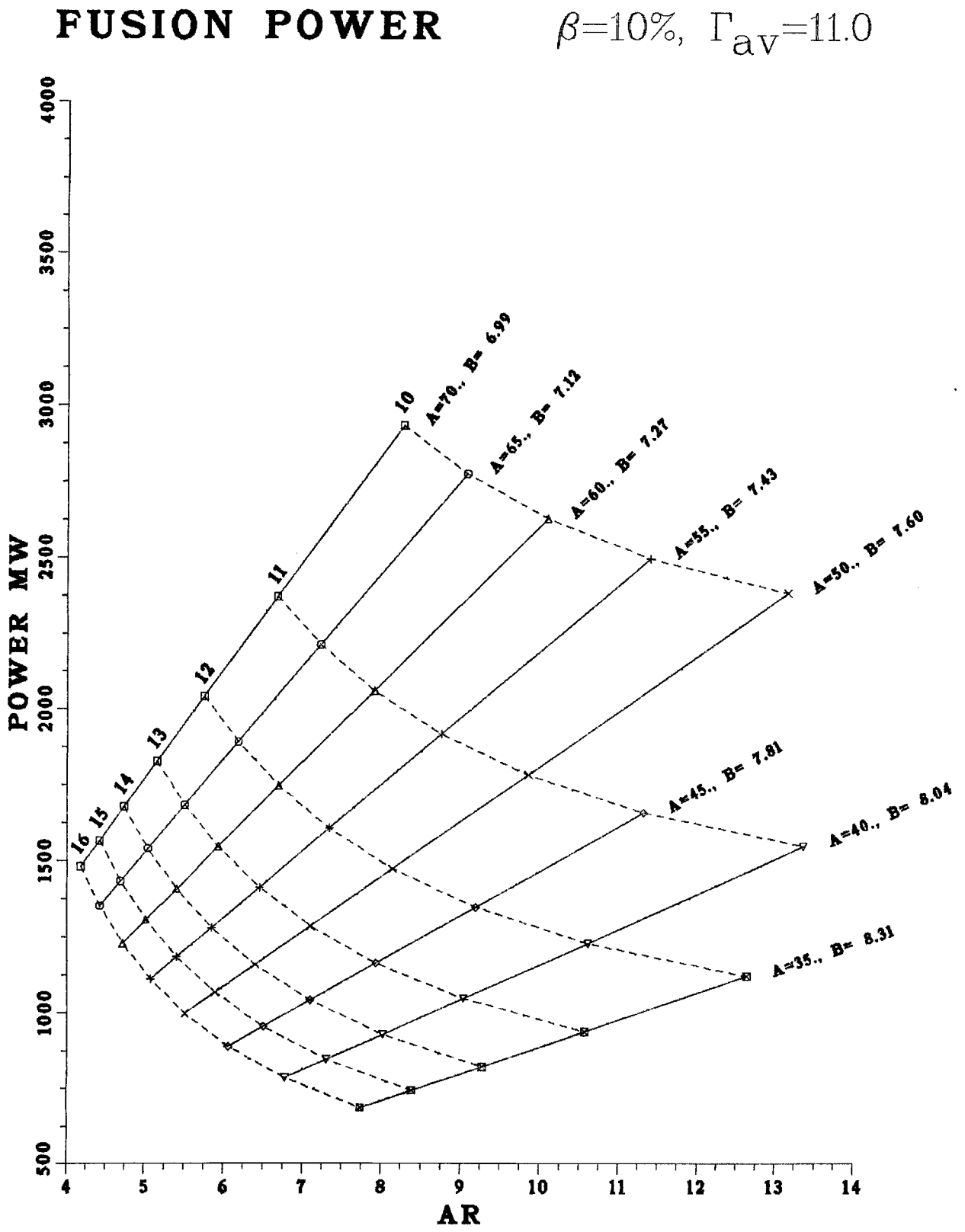

Fig. 4-10. P_f versus aspect ratio for Γ = 11 MW/m^2, β = 10%.

the aspect ratio and the fusion power, keeping the plasma radius and the maximum field the same. Second, for the same aspect ratio and for the same fusion power, the increase in β would decrease the required maximum field at the TF magnet, and this can make the use of NbTi possible.

Finally, the reactor configurations at the lowest aspect ratio for the three values of β and for 11 MW/m^2 neutron loading are shown in Fig. 4-11 to 4-13 together with major parameters. The complete parameters for the three cases are given in Table 4-2.

Table 4-2. Reactor Parameters

	Base Case	Low β	High β
β	0.08	0.06	0.1
Major radius (m)	3.239	3.848	2.923
Plasma radius (m)	0.7	0.7	0.7
Aspect ratio	4.627	5.497	4.176
Plasma shape (triangularity)	0.3	0.3	0.3
Elongation	1.6	1.6	1.6
Safety factor	2.0	2.0	2.0
Scrape off layer (m)	0.06	0.06	0.06
Z_{eff}	1.5	1.5	1.5
Z_{imp}	8.	8.	8.
Field on axis (T)	7.816	9.025	6.991
Ave. ion temperature (keV)	13.	13.	13.
Ave. electron temperature (keV)	13.	13.	13.
Plasma-current (MA)	7.293	6.847	7.461
β poloidal	2.003	2.273	1.915
Ion density ($/m^3$)	4.07E+20	4.07E+20	4.07E+20
Electron density ($/m^3$)	4.38E+20	4.38E+20	4.38E+20
$n\tau$ (s/m^3)	1.78E+20	1.78E+20	1.78E+20
τ_e (s)	0.407	0.407	0.407
Plasma edge neutron load (MW/m^2)	11.	11.	11.
Inboard peak neutron load (MW/m^2)	10.	NR*	NR*
Fusion power (MW)	1640.	1948.	1480.

*NR = Not Reported

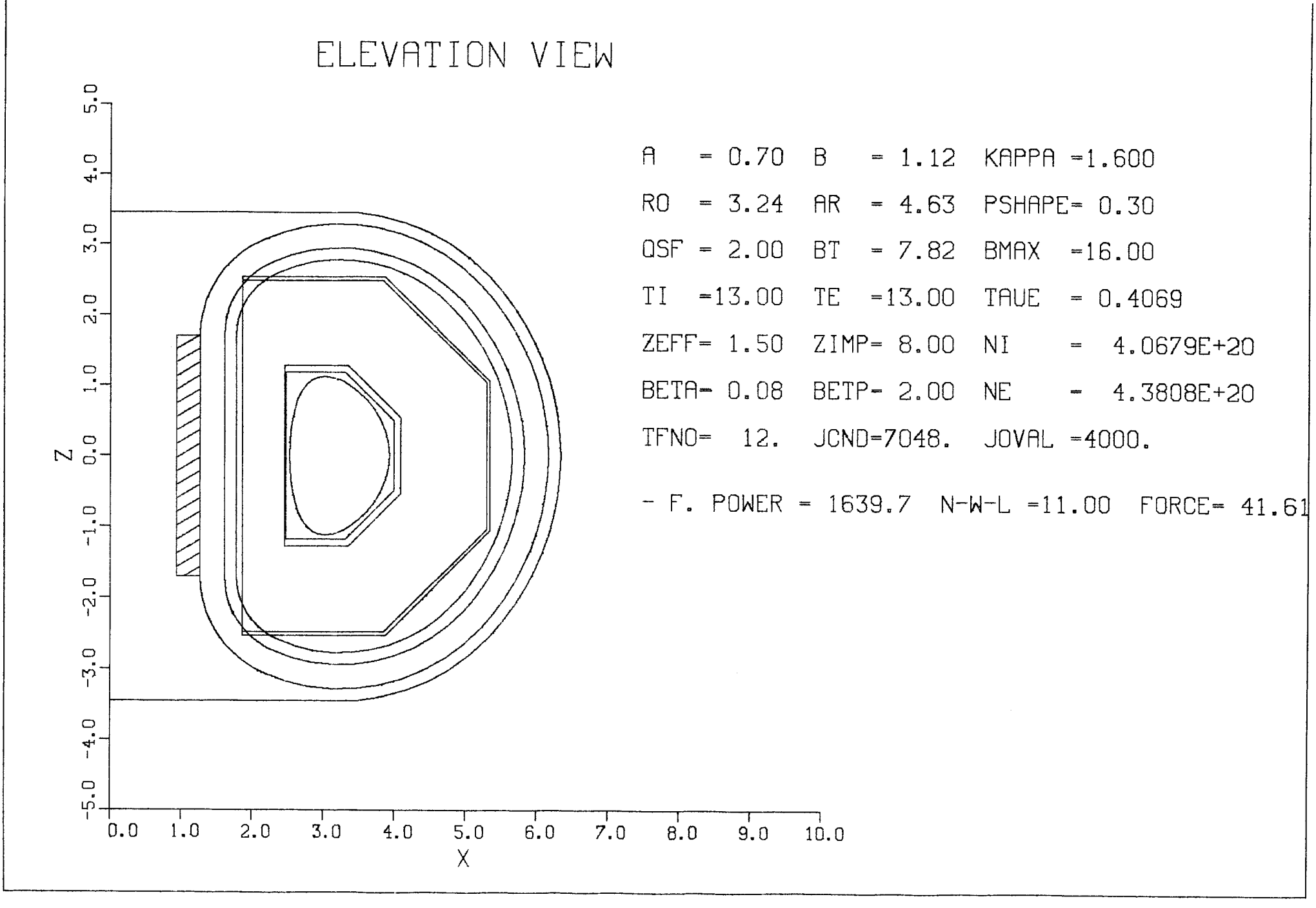

Fig. 4-11. (a) Reactor view for Γ = 11, β = 8%, $\bar{J}$ = 4000 A/cm^2.

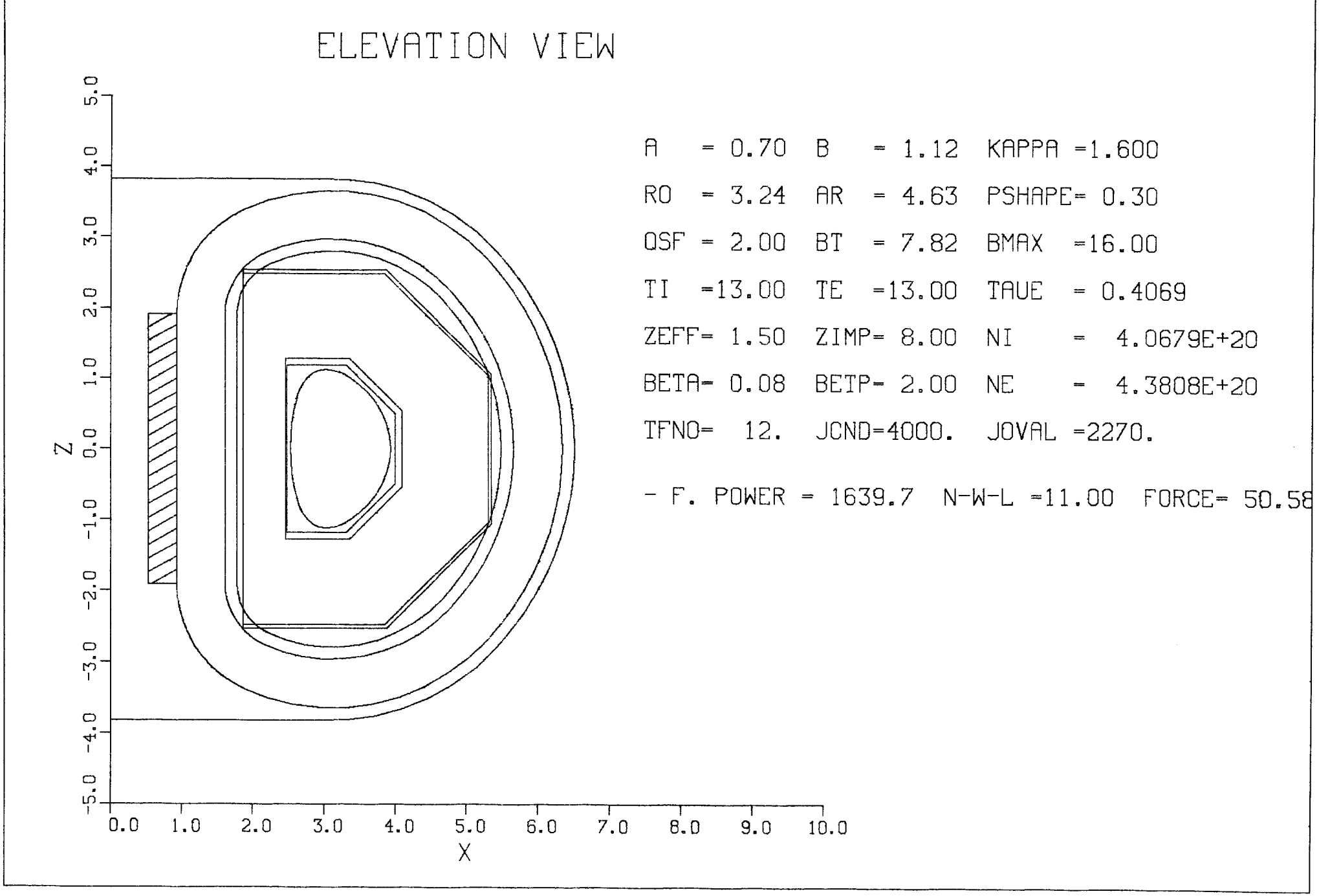

(b) Reactor view for $\Gamma = 11$, $\beta = 8\%$, $\bar{J} = 2000$ A/cm^2.

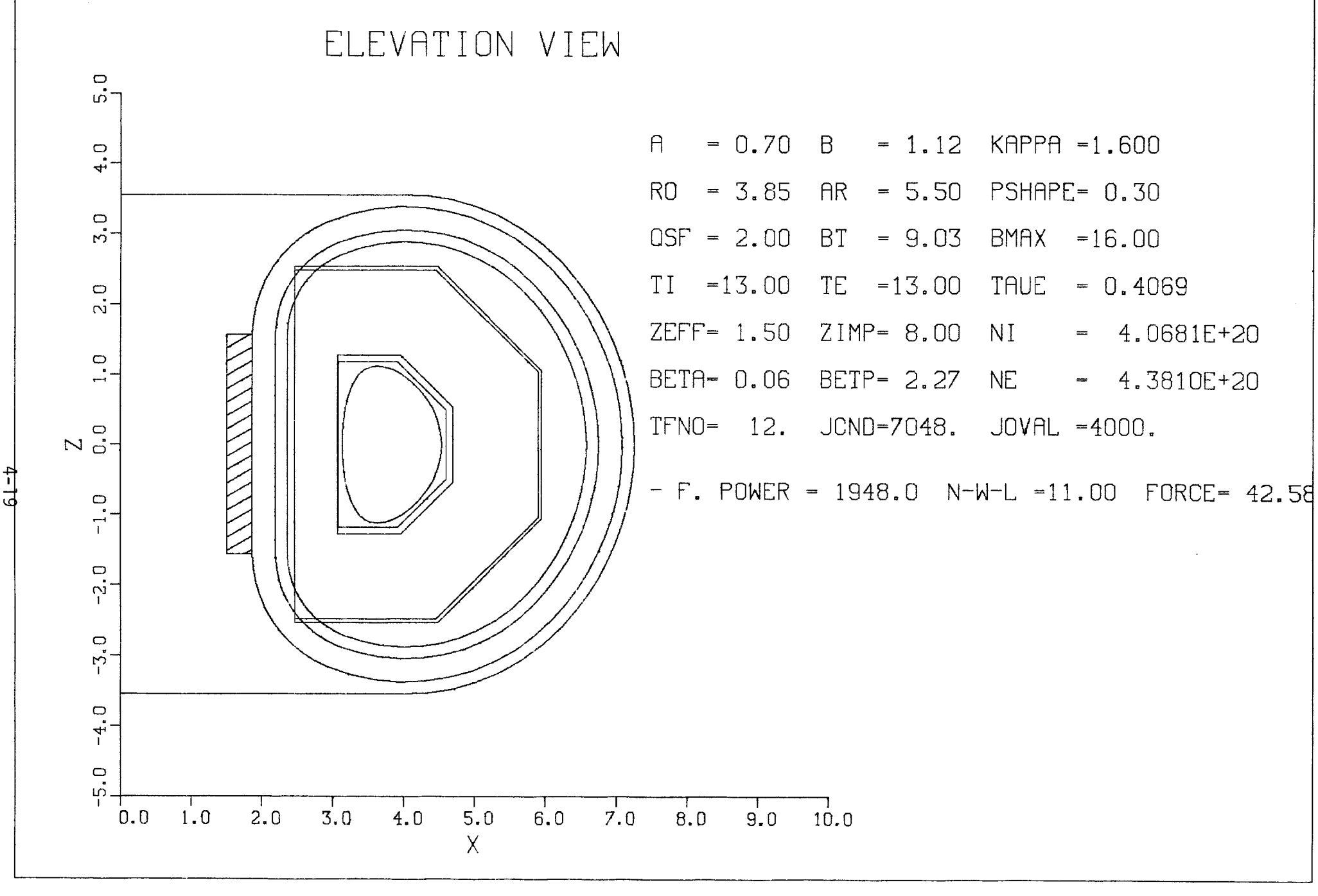

Fig. 4-12. Reactor view for Γ = 11, β = 6%.

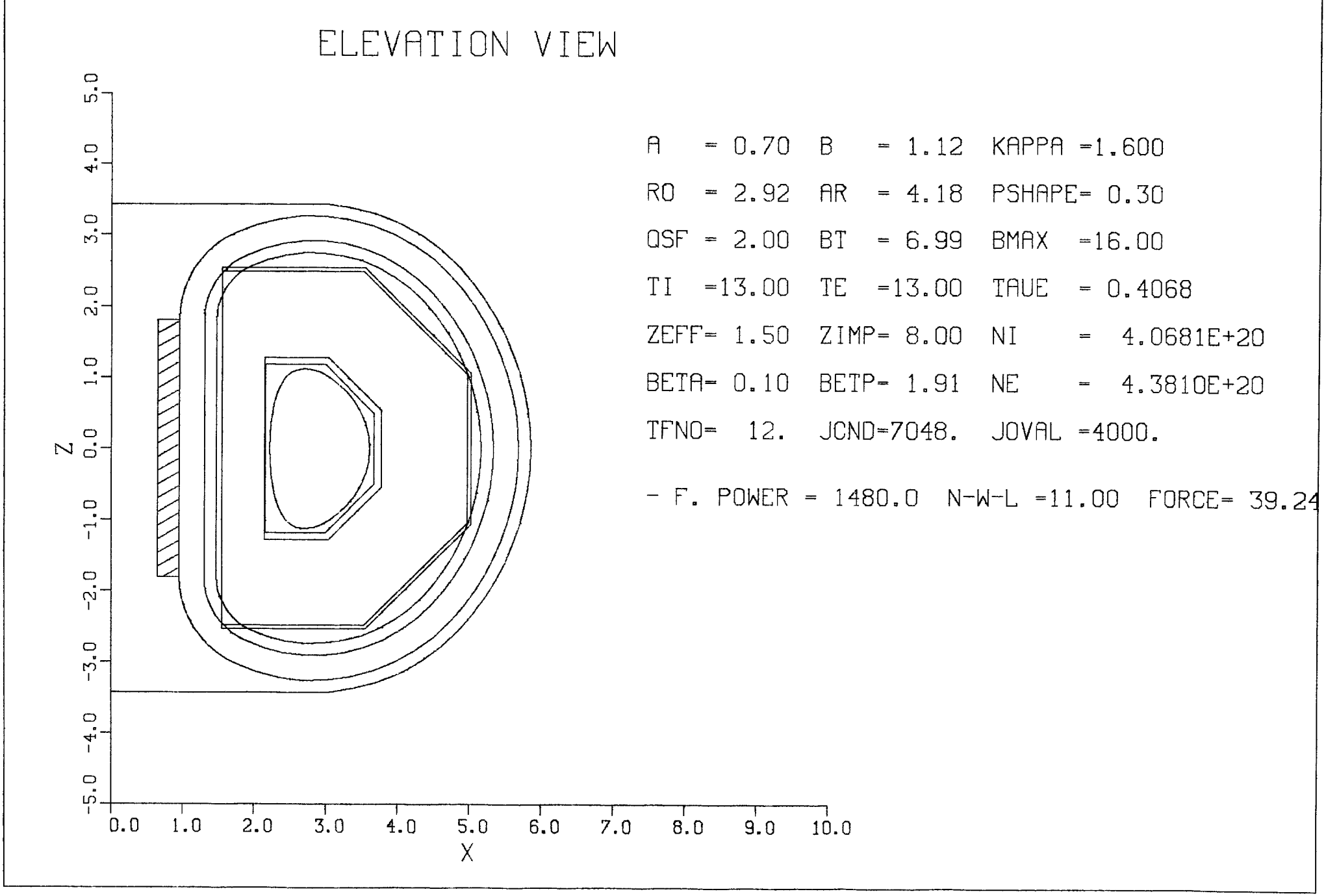

Fig. 4-13. Reactor view for β = 10%.

5. Breeding Blanket Design

In a compact tokamak, with a high fusion power density that requires large magnetic fields on the plasma axis, it is essential to reduce the space between the plasma and the TF coil in the inboard side of the torus. A breeding blanket and a magnet shield are usually used in this space. Since the breeding blanket is not an effective neutron shield, it is preferable to replace it by a more effective shield that reduces the space required for adequate magnet protection. Furthermore, the compactness makes it difficult to maintain or replace an inboard blanket. In this study, we investigate the possibility of obtaining an adequate overall tritium breeding ratio without breeding in the inboard side.

Proper choice of the material used in the inboard side is essential. Materials that provide large neutron reflection are required to enhance tritium breeding in the outboard breeding blanket. Calculations were performed to compare the ability of the different materials to reflect neutrons. The albedo, which is the measure of the number of neutrons, regardless of their energy, reflected from the inboard shield per 14.1 MeV incident neutron was calculated. Values of 1.03, 0.87, and 0.62 were obtained for tungsten, stainless steel and graphite, respectively. Micklich and Jassby[1] obtained values of 0.42 and 0.43 for B_4C and H_2O, respectively. The spectrum of neutrons reflected from steel and tungsten are very close while harder spectra are obtained from B_4C and softer spectra from water. In these calculations, no allowance was made for the required coolant and structure. Furthermore, the theoretical densities were used for the different materials. However, these results indicate that tungsten gives the best neutron reflection. Although using neutron multipliers on the inboard surface can yield larger reflection

(albedo values of 1.32 and 1.23 were calculated for Pb and Be, respectively[1]), neutron multiplication will require a larger inboard shield. Magnet shield optimization discussed in Chapter 3 indicated that the smallest shield thickness can be obtained when tungsten is used in front followed by a small layer of TiH_2 in the back. The use of this shield will help also the neutron reflection and tritium breeding in the outboard blanket. We also calculated the albedo for natural liquid lithium and $Li_{17}Pb_{83}$ in which the lithium is enriched to 90% ^6Li. The values obtained are 0.85 and 1.14, respectively. This implies that the reflection from the outboard blanket into the inboard shield is larger for a LiPb blanket than for a Li blanket. This indicates that the overall tritium breeding ratio (TBR) is more sensitive to the breeding blanket coverage fraction when LiPb is used.

In order to assess the possibility of achieving an adequate overall TBR without inboard breeding, several three-dimensional calculations were performed for a reference design with self-cooled Li (natural) and $Li_{17}Pb_{83}$ (90% ^6Li) blankets. In this design, the plasma has a major radius of 3 m, a minor radius of 0.5 m and an elongation of 1.6. A 10 cm thick scrape-off zone was allowed between the plasma boundary and the first wall at the midplane. A 0.5 cm thick HT-9 first wall was considered. A 60 cm thick shield with the optimum composition obtained from the shield optimization analysis was used in the inboard side. This shield consists mainly of a 54 cm thick tungsten zone (80 v/o W (0.9 d.f.), 10 v/o Fe-1422, and 10 v/o H_2O) followed by a 6 cm thick layer of TiH_2. The outboard blanket thickness is 80 cm and consists of 90 v/o breeder and 10 v/o HT-9. The breeding blanket coverage fraction in this model is ~ 80%. A 25 cm thick reflector consisting of 95 v/o 316 SS and 5 v/o H_2O was included in the model. The outboard shield and TF coil were not included

in the model as neutron reflection from them will have negligible impact on tritium breeding in the blanket. In order to investigate the effect of the limiter on the overall TBR, a bottom limiter, which was found to have less impact on TBR in a Li_2O system than a midplane limiter,[2] was included in the model. The limiter plate is 40 cm wide and extends toroidally around the entire chamber. It consists of 1 cm thick carbon tile and a 2 cm thick copper plate (60 v/o Cu and 40 v/o H_2O). The limiter base is made of 85 v/o 316 SS and 15 v/o H_2O and is 27 cm wide and 10 cm thick. The vacuum duct width is 20 cm. The continuous energy MCNP Monte Carlo code[3] was used in the calculations. Figure 5-1 gives a cross section of the geometrical model used in the Monte Carlo calculations. Two thousand histories were used yielding statistical uncertainties of less than 1% in the calculated overall TBR.

Calculations were performed for the case with no limiter for the Li and LiPb blankets using neutron cross section data based on both the ENDF/B-IV and ENDF/B-V evaluations. The results are given in Table 5-1. It is clear that the overall TBR in the LiPb case is larger than unity by a comfortable margin that allows for data uncertainties, calculational deficiencies and blanket penetrations. The ENDF/B-V data give slightly lower $^6Li(n,\alpha)t$ cross sections in the energy range around the 252 keV resonance. This reaction dominates tritium breeding in a LiPb system. Using the ENDF/B-V data was found to result in ~ 2% reduction in TBR. This yields a value of 1.24 which is still comfortably large.

Although the ENDF/B-IV and V data for ^7Li are identical, strong doubts about the validity of the $^7Li(n,n'\alpha)t$ cross section have been expressed.[4-7] Lowering the cross section by 15-20% has been suggested. This is expected to have a larger impact on the TBR in the Li case as ~ 36% of tritium is produced

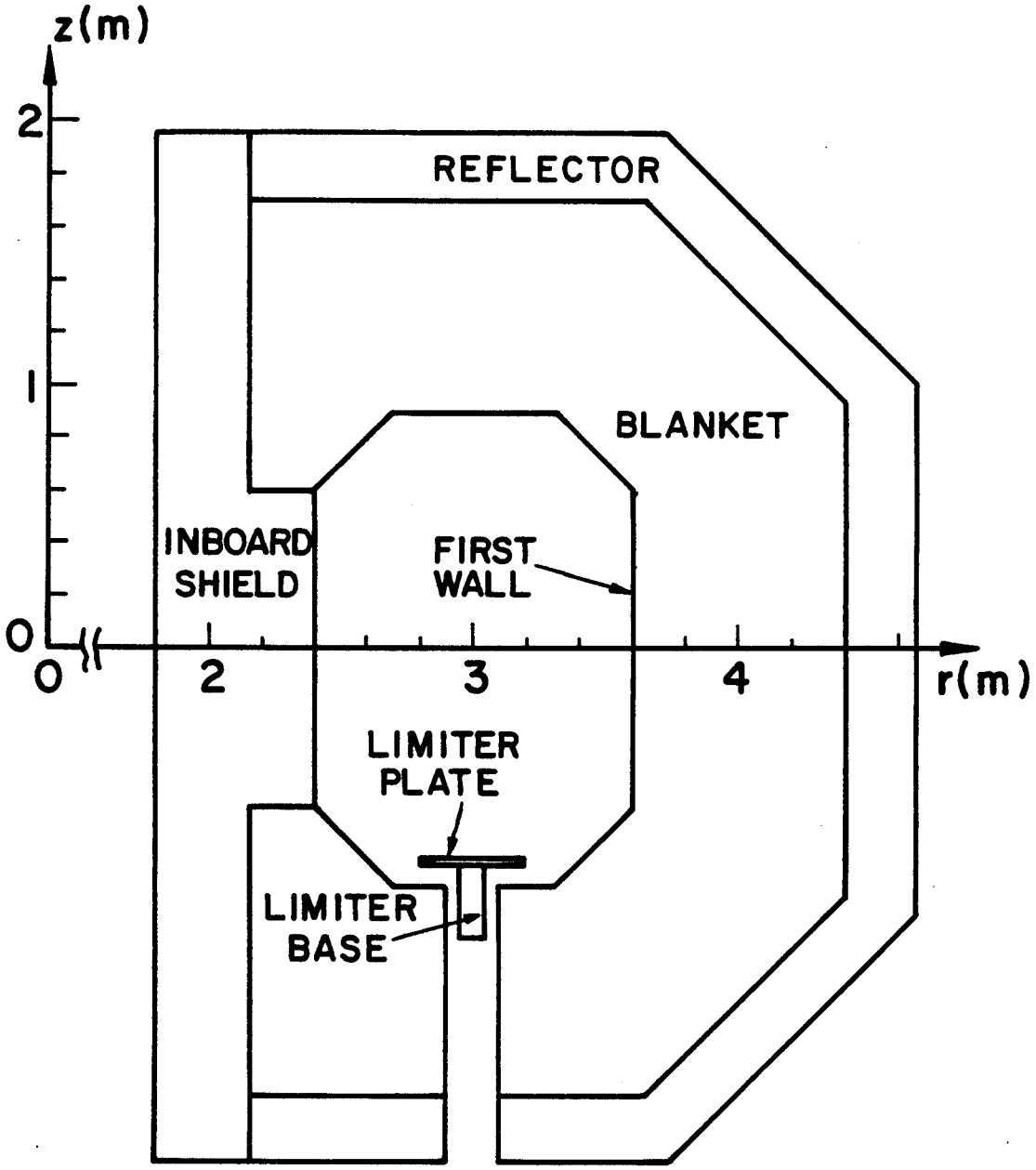

Fig. 5-1. Geometrical model used in the Monte Carlo calculations.

Table 5-1. Tritium Breeding Results Obtained Using ENDF/B-IV and V Data with No Inboard Breeding and No Limiter

	Li Blanket			LiPb Blanket	
	ENDF/B-IV	ENDF/B-V	ENDF/B-V with New ^{7}Li Data	ENDF/B-IV	ENDF/B-V
$^{6}Li(n,\alpha)t$	0.747	0.732	0.794	1.264	1.338
$^{7}Li(n,n'\alpha)t$	0.426	0.426	0.382	0.002	0.002
TBR	1.173	1.158	1.176	1.266	1.240

via this reaction. Different researchers use a correction factor of ~ 0.85 to adjust the tritium production in ^{7}Li.[8,9] Not only does the ^{7}Li $(n,n'\alpha)t$ cross section decrease in the new experimental results but the spectrum of emitted secondary neutrons is represented by a discrete spectrum rather than a continuum.[5] Comparing the spectra, we observe that the new experimental results give softer secondary neutron spectra. More low energy neutrons ($E \lesssim 2$ MeV) are produced in the $^{7}Li(n,n'\alpha)t$ reaction. Since these neutrons are available for breeding tritium via the $^{6}Li(n,\alpha)t$ reaction which has a $1/\sqrt{E}$ cross section, using the new ^{7}Li data is expected to give larger tritium production from ^{6}Li. The net effect on the total TBR is design dependent. The effect of ^{6}Li dominates when thick blankets with small structure content are used. A LANL evaluation for the ^{7}Li cross section data based on the new experimental data was included in a modified ENDF/B-V data file for MCNP. We used this data to investigate the impact on the overall TBR in the Li case. The results are included in Table 5-1. The tritium breeding via $^{7}Li(n,n'\alpha)t$ decreased by ~ 11% while tritium breeding by $^{6}Li(n,\alpha)t$ increased by ~ 8%.

This results in nearly the same TBR as that obtained from ENDF/B-IV. This is consistent with the results of Gohar (Section VIII.1.5 of Ref. 9) which indicated a reduction of 10-11% in the $^{7}Li(n,n'\alpha)t$ reaction and net decreases in TBR of 7.2 and 4.6% in 40 and 60 cm thick Li blankets, respectively, compared to the ENDF/B-IV results.

Finally, the impact of using the limiter system on the overall TBR in the Li system was investigated. Using the geometrical model of Fig. 5-1 and the ENDF/B-V data with the new ^{7}Li evaluation, we obtained the results given in Table 5-2. The results for the case with no limiter are included for the purpose of comparison. The effect of the limiter reduces the TBR by ~ 4%. The resulting TBR of 1.129 is still larger than unity by a comfortable margin.

We conclude from this analysis that a highly enriched LiPb blanket has the highest breeding potential. A natural liquid lithium blanket can still provide adequate breeding even when limiter penetrations and the new Li data are considered. There is no need for using neutron multipliers which add complexity and cost.

The final design has a major radius of 3.24 m and a minor plasma radius of 0.7 m. The reactor configuration is shown in Fig. 5-2. A total space of 1.5 m is available in the outboard side for the blanket, reflector, and shield. Hence a 45 cm thick shield can be used. Using a shield that consists

Table 5-2. Effect of Limiter on Tritium Breeding in the Li Blanket

	With Limiter	Without Limiter
$^{6}Li(n,\alpha)t$	0.760	0.794
$^{7}Li(n,n'\alpha)t$	0.368	0.382
TBR	1.129	1.176

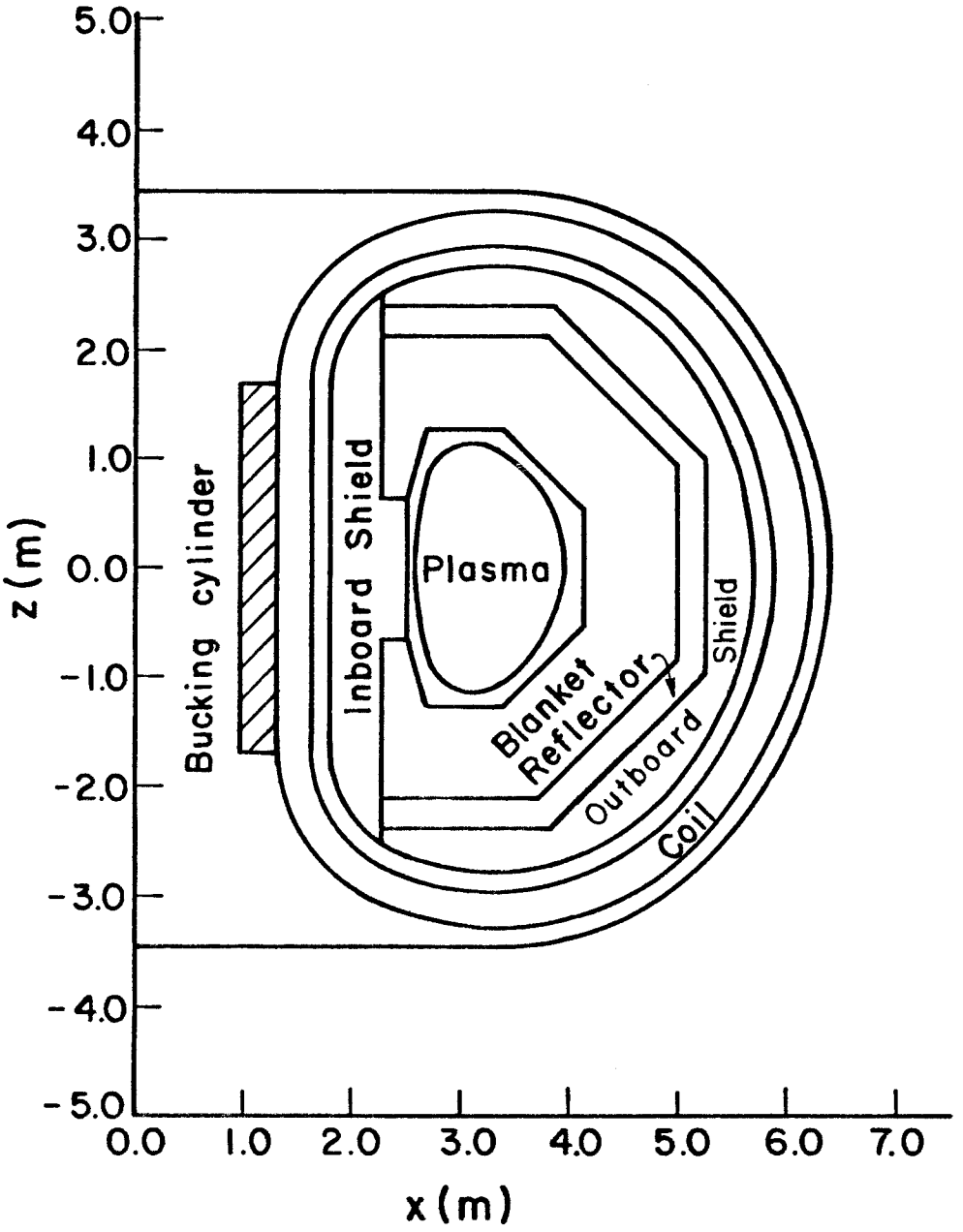

Fig. 5-2. Geometrical configuration of the final reactor design.

mainly of the manganese steel Fe-1422 yields peak radiation effects in the outboard section of the magnet that are more than two orders of magnitude lower than those in the inboard portion. The breeding blanket coverage remains the same yielding values of TBR close to those obtained in the previous calculations.

References for Chapter 5

1. B. Micklich and D. Jassby, Trans. Am. Nucl. Soc. 44, 144 (1983).
2. Y. Gohar, Trans. Am. Nucl. Soc. 44, 140 (1983).
3. "MCNP - A General Monte Carlo Code for Neutron and Photon Transport," LA-7396-M, Los Alamos National Laboratory (1981).
4. R. Herzing et al., Nucl. Sci. Engr. 60, 169 (1976).
5. H. Backmann et al., Nucl. Sci. Engr. 67, 74 (1978).
6. A. Hemmendinger et al., Nucl. Sci. Engr. 70, 274 (1979).
7. P. Young, Trans. Am. Nucl. Soc. 39, 272 (1981).
8. J. Jung and M. Abdou, Nucl. Technology/Fusion 4/2, 361 (1983).
9. M. Abdou et al., "Blanket Comparison and Selection Study Interim Report," ANL/FPP-83-1, Argonne National Laboratory (1983).

6. Summary of S/C Blanket and Shield Design

The purpose of this chapter is to briefly summarize the conclusions of Chapters 2-5 on the superconducting design option. Table 6-1 includes the main design parameters for the proposed system.

Table 6-1. Key Design Parameters for Shield and Blanket Designs in S/C High Field Tokamak Option

Parameter	Unit	Value
Plasma		
DT Power	MW_{th}	1640
Major Radius	m	3.24
Field on Axis	tesla	7.8
$\langle\beta\rangle$	%	8
Γ_n^{ave}	MW/m^2	10.33
Γ_n^{Peak} (Inboard)	MW/m^2	10
Inboard		
Total Thickness	cm	60
Composition	---	W/TiH_2 Borated Water Fe 1422
Inboard S/C Magnet (Peak)		
Nuclear Heating	mW/cm^3	2.2
dpa Cu Stabilizer	dpa/24 FPY	0.029
dpa Nb_3Sn	dpa/24 FPY	~ 0.02
Dose - Electrical Insul.	Rad/24 FPY	7.4×10^{10}
Outboard Blanket		
Thickness	cm	80
Structure	---	HT-9
Breeding Ratio	---	1.13 (Li) 1.19 ($Pb_{83}Li_{17}$)

The first major conclusion is that it is possible to shield the inboard portion of a S/C TF coil from a 10 MW/m^2 peak wall loading for 24 FPY's with only 60 cm of an optimized configuration. It was also shown that the additional shield thickness to shield against a 10 MW/m^2 vs. a 1 MW/m^2 wall loading is only 14 cm of the optimized shield design.

The second major conclusion is that it is possible to breed entirely on the outboard side of a tokamak with the optimized inboard non-breeding shield. The overall breeding ratio accounting for losses via a pumped limiter is 1.13 for Li and 1.19 for a $Pb_{83}Li_{17}$ self-cooled HT-9 structure design. This conculsion is particularly important in view of the difficulty in maintaining the inboard side of a tokamak and should have an important impact on compact tokamak power reactor designs.

The third important conclusion is that even with a high field/high wall loading design, the power level will be in the 1600 MW range at even optimistic beta/aspect ratio combinations. This is somewhat disappointing from the desirability to design low <u>total</u> power, high power density tokamaks. The objective of a low total power design was to reduce the total cost of a device for nearer term application.

7. Hybrid Coils

7.1 Introduction

Hybrid coil systems are defined as those in which normal conducting coils are used in conjunction with superconducting coils to produce the required magnetic fields. There are basically two ways in which normal coils can be used in a fusion power reactor: as supplementary coils, to enhance or supplement the field on the plasma axis, and as trimming or field shaping coils.

As supplementary coils, normal magnets can be used to replace a part of, or add to the field supplied by the superconducting magnet system. If for example, a field is required that is slightly in excess of that capable of being produced with NbTi, a supplementary normal conducting magnet might be considered instead of using the more brittle and more costly Nb_3Sn. This is illustrated in Fig. 7-1. Further, if one wishes to exceed magnetic fields which present conventional superconductors are capable of producing (16 T for Nb_3Sn), then this also can be done with supplementary normal coils, as is shown in Fig. 7-2. A good example of that is in the barrier coils of tandem mirrors in which fields as high as 24 T are sometimes needed.[1]

Because normal conductors are less susceptible to radiation damage (except for the insulators), they can be placed close to the plasma with minimal shielding. In this way the circumference is not large and I^2R losses are kept to a minimum. However, as supplementary coils for toroidal fields in tokamaks, for example, placing the coils close to the plasma increases the field inhomogeneity, since the coils have to be discreet. Thus, the problem of maximum field variation at the plasma edge has to be taken into account.

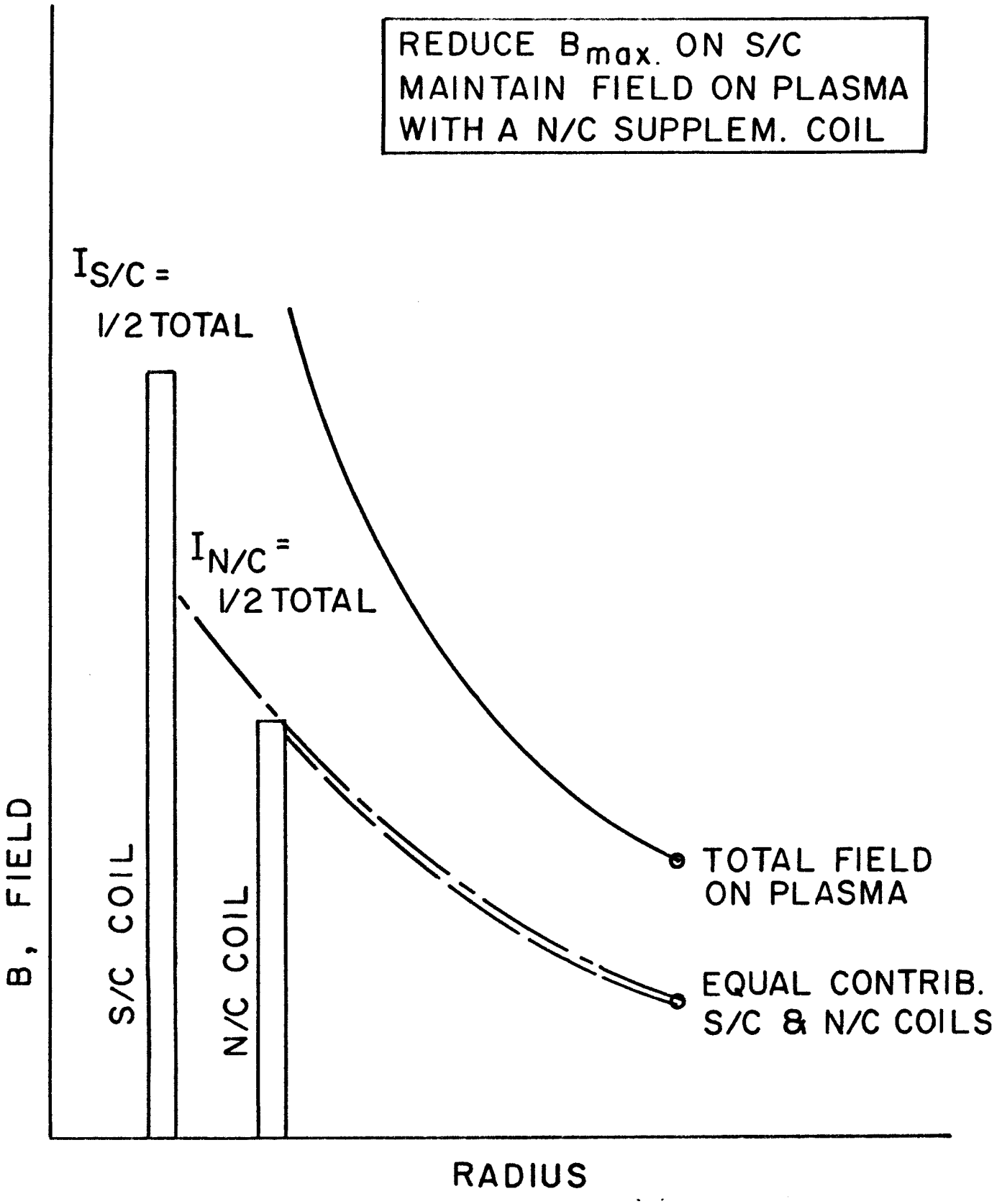

Fig. 7-1. The radial variation of the magnetic field in the toroidal configuration when normal conducting (N/C) coils are used to reduce the maximum field generated by the superconducting coil (S/C).

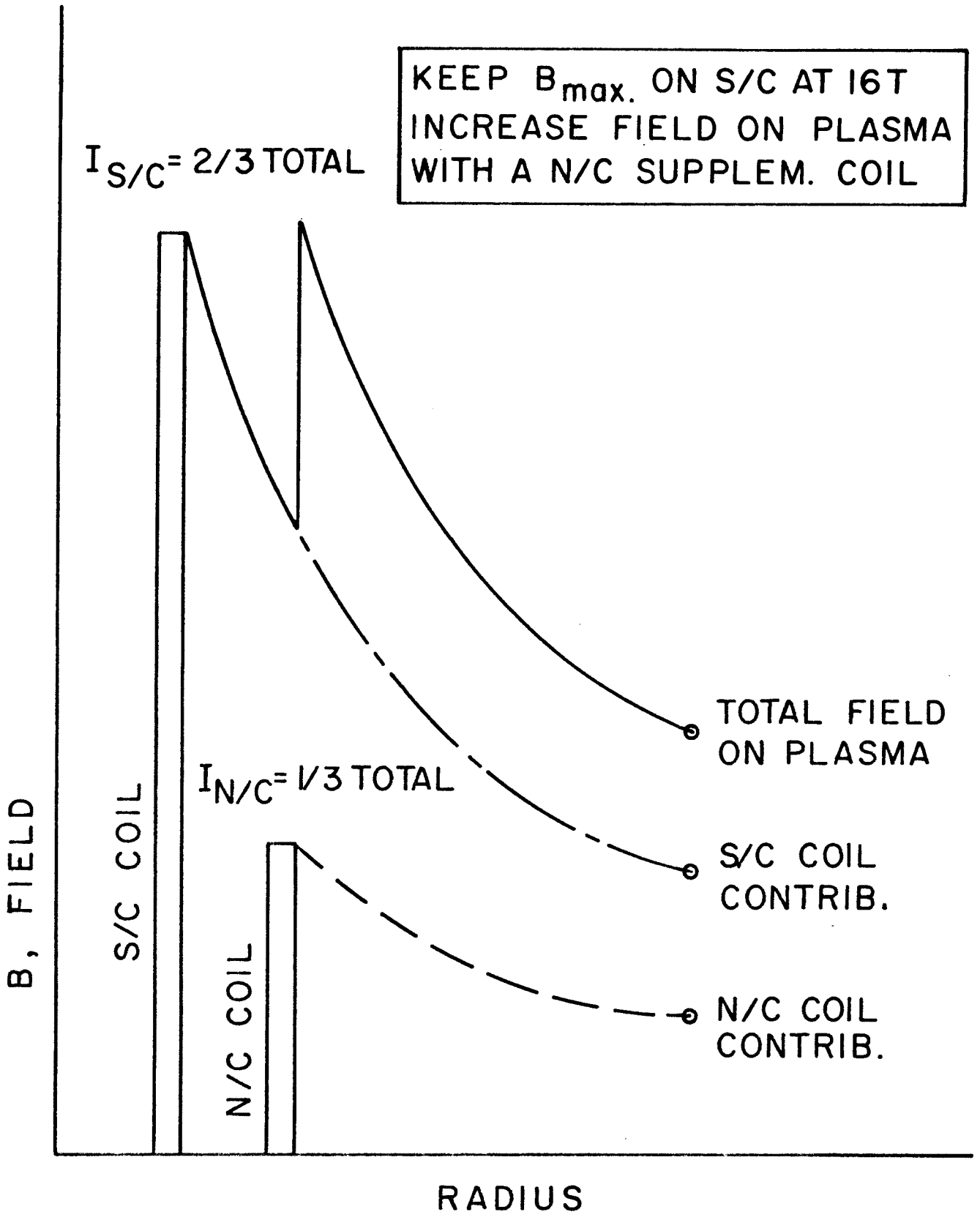

Fig. 7-2. The radial variation of the magnetic field when normal conducting (N/C) coils are used to supplement superconducting (S/C) coils.

As trimming or field shaping coils, the normal conducting magnets could, but need not, circumvent the plasma. As such, they can add or subtract flux in strategic places in order to perform field shaping. Saddle coils have been proposed for this purpose.[2]

7.2 Power Requirements

In this study we have only considered the supplementary hybrid coil systems. Two cases have been considered and are illustrated in Fig 7-3. In the first (Case 1A) the normal conducting coil follows the inner contour and hugs the inner surface of the superconducting TF coil. In the second case (Case 2A), the normal coil is placed at the first wall on the inboard side, which is 60 cm from the superconducting coil edge, but on the outboard side it stays at the same distance and again follows the contour of the S/C coil. In other words, it does not stay at the first wall on the outboard side. In principle, the normal coil could have stayed at the first wall on the outboard side too, but then the issue of field ripple at the plasma edge would have had to be addressed.

To further reduce the I^2R losses, the two cases were expanded to include a lower current density by a factor of two on the outboard side. This would entail a graded conductor in which 60% of the circumference has a conductor with twice the area of that on the inboard side. These cases are designated 1B and 2B. Table 7-1 gives the parameters used in calculating the ohmic heating in the four cases considered.

The power losses for the four cases of normal coils were calculated parametrically where a range of 0-30% of the total ampere turns in the S/C coil was replaced with the normal coil. The results are given in Table 7-2.

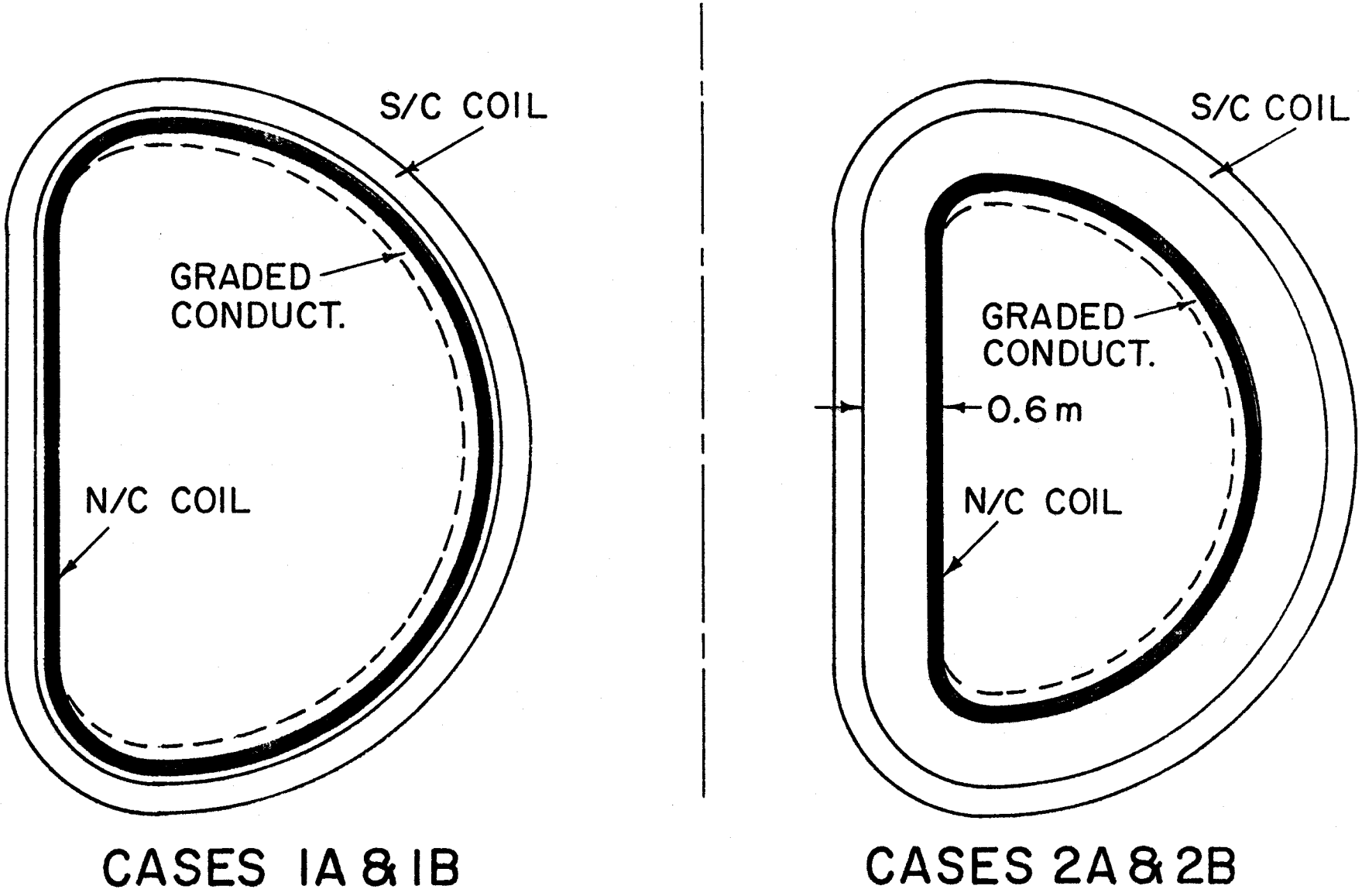

Fig. 7-3. Schematic of the normal coil placements in the superconducting TF coil. Cases 2A and 2B place the N/C coil at the first wall.

Table 7-1. Parameters Used in Calculating Power Losses

Horizontal inner bore of S/C TF coil (m)	4
Vertical inner bore of S/C TF coil (m)	5.8
Current in S/C coil (MA)	8.54
Material of normal cond.	1/2 hard copper
Block current density (A/cm^2)	2000
Cond. current density (A/cm^2)	3180
Cond. current (kA)	20
Dimension of conductor + insulation (cm)	5 x 2
No. of 1 cm diameter cooling holes	3
Area of Cu in conductor (cm^2)	6.28
Resistivity of Cu at 150°C (Ω m)	2.5×10^{-8}

Table 7-2. Power Losses in Normal Coils for the Whole Reactor

% of Current in Normal Coil	Case 1A (MWe)	Case 1B (MWe)	Case 2A (MWe)	Case 2B (MWe)
10	127.7	89.4	96.9	67.8
15	190.6	133.4	144.4	101.1
20	252.5	176.7	191.0	133.7
25	313.9	219.7	237.1	166.0
30	374.4	262.1	282.3	197.6

It is clear from Table 7-2 that even replacing or enhancing 10% of the field at the plasma with normal conductors requires an enormous amount of power. In Case 2B, where the normal coil is at the first wall on the inboard side but follows at 60 cm from the S/C coil on the outboard side and has a

graded conductor with a current density over 60% of its circumference one half that on the inboard side, the power required is ~ 68 MW. For a 1650 MW_{th} reactor with a net electric power of say 550 MW_e, this amounts to ~ 12%. To replace or enhance the field by 30%, the power goes up to almost 40%.

In conclusion it is evident that the use of hybrid coils in TF magnets of tokamaks requires an excessive drain on the electric output of the system. This conclusion may not be true for extremely high energy density systems in which the neutron wall loading is much higher than 10 MW/m^2.

7.3 Radiation Effects and Shielding Requirements

In view of the fact that the peak neutron wall loading at the inboard shield is 10 MW/m^2, the normal magnet is operating in a severe radiation environment. In this magnet, there is concern with both electrical and mechanical degradation of the ceramic insulation and the electrical resistivity of the copper conductor due primarily to neutron induced-transmutations. An additional potential problem is radiolytic decomposition of the water coolant leading to corrosion product formation. Among the mechanisms mentioned above, only one was found as lifetime limiting for the normal coil,[1] namely the swelling in the ceramic insulator.

There are common ceramic insulators that are used for the insulation in the normal conducting coils, such as alumina (Al_2O_3), magnesium oxide (MgO), and spinel ($MgAl_2O_4$). The ceramics are available in a compacted powder or solid form. A reasonable experimental data-base on swelling exists for these materials,[3-5] and the solid spinel appears to offer the lowest degree of swelling among its class of cubic ceramic insulators. This factor dictated the choice of spinel insulator for the normal magnet. A stress analysis shows that 3 vol.% neutron induced-swelling in spinel can be accommodated in the

magnet structure without causing stress problems. Therefore, with the rather conservative assumption that the harder fusion spectrum will enhance the swelling rate by a factor of two over the fast fission irradiation, the fluence limit to the spinel insulation is 4 x 10^{22} n/cm^2 for 3 vol.% swelling. In fact, the fluence limit is directly proportional to the swelling in the insulators and a smaller or cheaper normal magnet can be built if the magnet designer can tolerate more swelling in the spinel.

The one-dimensional calculations result in a peak neutron fluence (for E_n > 0.1 MeV) in the spinel of 1.2 x 10^{23} n/cm^2 per full power year (FPY) of operation for the case where the normal coil is positioned with no intervening W-shield between its coil case (0.02 m thick) and the first wall. This was for a 10 MW/m^2 neutron wall loading at the inboard shield. The neutron fluence indicates that the normal coil needs to be replaced every 0.33 FPY due to this mechanism alone. In order to achieve a practical change-out period for the normal magnet, such as 3 FPY, it is recommended that some shielding be introduced in front of the normal coil and/or more swelling in the insulator be allowed. Our calculations indicate that 0.2 m of W-shield would increase the change-out period to 3 FPY for 3 vol.% swelling in the spinel. On the other hand, if one allows 10 vol.% swelling in spinel as a design tolerance, there is a need for only 0.1 m of W-shield for the normal magnet to be replaced every 3 FPY.

In the calculations the normal magnet composition was taken as 64 vol.% Cu, 24 vol.% spinel, and 12 vol.% H_2O. A total W and TiH_2 shield thickness of 0.6 m was found to adequately protect the inboard side of the S/C magnet (see Chapter 3). Clearly, the normal magnet materials are not as effective as the W in attenuating the radiation. Therefore, additional shield to protect the

S/C magnet should be provided in the reactor design of the hybrid coils. The results show that replacing 0.05 m of W-shield by the normal magnet composition would increase the fast neutron fluence in the S/C magnet by ~ 16%. This means that if 0.3 m thick normal magnet is used the total W-TiH_2 shield and normal magnet thicknesses should be 0.65 m to satisfy the design limits for the S/C magnet.

References for Chapter 7

1. "Mirror Advanced Reactor Study (MARS) - Report," UCRL-53333-83, Lawrence Livermore National Laboratory (to be published in 1983).

2. B. Badger et al., "NUWMAK, A Tokamak Reactor Design Study," UWFDM-330, Fusion Engineering Program, UW-Madison, Wisconsin, March 1979.

3. J.H. Schultz, "Design Practice and Operational Experience of Highly Irradiated, High Performance Normal Magnets," J. of Fusion Energy 3, (Nov. 1983).

4. R.E. Gold et al., "Materials Technology for Fusion: Current Status and Future Requirements," Nuclear Technol./Fusion 1, 169 (1981).

5. G.F. Hurley, J.C. Kennedy and F.W. Clinard, "Structural Properties of MgO and $MgAl_2O_4$ After Fission Neutron Irradiation Near Room Temperature," LA-UR-81-2078, Los Alamos National Laboratory (1981).

8. Future Work

This project has uncovered some very interesting topics which need to be examined in more detail. These topics fall into three categories:

A. Tokamak Design Code Related

B. Reassessment of Radiation Damage Limits for S/C Magnets

C. Mechanical Design of Inboard Shield and Outboard Breeding Blankets.

Resolution of these issues could result in even more realistic compact tokamak designs.

A. Tokamak Design Code. The present FEDC/TSC code does not have the capability to incorporate spatial wall loading variations. It also does not contain provisions for realistic iterative inboard shield calculations. Such revisions are not only desirable from the perspective of "traditional" tokamaks but they will be very important if "bean" shaped plasmas are to be utilized. At the present time the poloidal variation and optimized shield calculations must be done separately and then inserted into the TSC/FEDC code.

B. Reassessment of Radiation Damage Limits for S/C Magnets. It is obvious that the exact level of allowable neutron wall loading depends on several radiation damage limits in the magnets. A systematic study of the sensitivity of magnet lifetime to these limits (taking into account that each limit requires a different "optimized" shield) needs to be performed. Once the high sensitivity parameters are identified, interaction with the materials community is required to "push" the present design limits to higher values. This will involve outlining specific experimental data which is required and suggesting material to be tested.

C. Mechanical Design of Inboard Shield and Outboard Breeding Blankets. The present study has suggested the homogenized blanket and shield concepts that could fulfill the design objectives. In order to further validate these designs, thermal hydraulic and stress analyses need to be performed. Such analyses need not proceed to the "nuts and bolts" stage, but can be conducted at the level of conceptual designs which incorporate the neutronic analysis already performed in the present study. Once such designs were performed and accepted, one could then proceed (in another study) to a preconceptual reactor stage.

Acknowledgment

Support for this work has been provided by the U.S. Department of Energy.